UNIVERSIDAD DE CONCEPCIÓN

Centro de Investigación en Ingeniería Matemática (CI^{2}MA)

A posteriori error analysis of a mixed finite element method for the stationary convective Brinkman–Forchheimer problem

Sergio Caucao, Gabriel N. Gatica,
Luis F. Gatica

PREPRINT 2024-18

SERIE DE PRE-PUBLICACIONES

A posteriori error analysis of a mixed finite element method for the stationary convective Brinkman–Forchheimer problem*

Sergio Caucao† Gabriel N. Gatica‡ Luis F. Gatica§

Abstract

We consider a Banach spaces-based mixed variational formulation that has been recently proposed for the nonlinear problem given by the stationary convective Brinkman–Forchheimer equations, and develop a reliable and efficient residual-based *a posteriori* error estimator for the 2D and 3D versions of the associated mixed finite element scheme. For the reliability analysis, we utilize the global inf-sup condition of the problem, combined with appropriate small data assumptions, a stable Helmholtz decomposition in nonstandard Banach spaces, and the local approximation properties of the Raviart–Thomas and Clément interpolants. In turn, inverse inequalities, the localization technique based on bubble functions in local L^p-spaces, and known results from previous works, are the main tools yielding the efficiency estimate. Finally, several numerical results confirming the theoretical properties of the estimator and illustrating the performance of the associated adaptive algorithm are reported. In particular, the case of flow through a 2D porous medium with fracture networks is considered.

Key words: convective Brinkman–Forchheimer equations, pseudoestress-velocity formulation, mixed finite element methods, Banach spaces, *a posteriori* error analysis, reliability, efficiency.

Mathematics subject classifications (2000): 65N30, 65N12, 65N15, 35Q79, 76R05, 76D07

1 Introduction

We recently introduced in [7] a Banach spaces-based mixed finite element method for the problem of fluid flow through highly porous media at higher Reynolds numbers, described by the stationary convective Brinkman–Forchheimer (CBF) equations in $\mathrm{R}^d, d \in \{2, 3\}$. There, besides the velocity, the pseudostress tensor is introduced as a further unknown of the system, thus yielding a mixed variational formulation consisting of a nonlinear perturbation of, in turn, a perturbed saddle point problem in a Banach spaces framework. In this way, and unlike the techniques previously developed for this model

*This research was supported by ANID-Chile through the projects Centro de Modelamiento Matemático (FB210005), Anillo of Computational Mathematics for Desalination Processes (ACT210087), and Fondecyt 11220393; by DI-UCSC through the project FGII 04/2023; by Grupo de Investigación en Análisis Numérico y Cálculo Científico (GIANuC^2), Universidad Católica de la Santísima Concepción; and by Centro de Investigación en Ingeniería Matemática (CI^{2}MA), Universidad de Concepción.

†GIANuC^2 and Departamento de Matemática y Física Aplicadas, Universidad Católica de la Santísima Concepción, Casilla 297, Concepción, Chile, email: scaucao@ucsc.cl.

‡CI^{2}MA and Departamento de Ingeniería Matemática, Universidad de Concepción, Casilla 160-C, Concepción, Chile, email: ggatica@ci2ma.udec.cl.

§GIANuC^2 and Departamento de Matemática y Física Aplicadas, Universidad Católica de la Santísima Concepción, Casilla 297, Concepción, Chile, and CI^{2}MA, Universidad de Concepción, Casilla 160-C, Concepción, Chile, email: lgatica@ucsc.cl.

in [6], no augmentation procedure needs to be incorporated into the formulation or into the solvability analysis. The resulting non-augmented scheme is then equivalently written as a fixed-point equation, allowing the application of recently established solvability results for perturbed saddle-point problems in Banach spaces, along with the well-known Banach–Nečas–Babuška and Banach theorems, to prove the well-posedness of the continuous and discrete systems. The finite element discretization involves Raviart–Thomas elements of order $k \geq 0$ for the pseudostress tensor and discontinuous piecewise polynomial elements of degree $\leq k$ for the velocity. Stability, convergence, and optimal *a priori* error estimates were also derived in [7].

It is well known that adaptive algorithms based on *a posteriori* error estimates are well suited to recover the loss of convergence orders in most standard Galerkin procedures, such as finite element and mixed finite element methods. This is particularly true when these methods are applied to nonlinear problems in the presence of singularities or high gradients in the exact solutions. In particular, this powerful tool has been applied to quasi-Newtonian fluid flows obeying the power law, which includes the CBF model. In this direction, we refer to [19], [20], [29], [9], and [6], for various contributions addressing this issue. Particularly, in [19] an *a posteriori* error estimator defined via a non-linear projection of the residuals of the variational equations for a three-field model of a generalized Stokes problem was proposed and analyzed. In turn, a new *a posteriori* error estimator for a mixed finite element approximation of non-Newtonian fluid flow problems was developed in [20]. This mixed formulation, like finite volume methods, possesses local conservation properties, namely conservation of momentum and mass. Later on, *a posteriori* error analyses for the aforementioned Brinkman–Darcy–Forchheimer model in velocity-pressure formulation were developed in [29]. Specifically, two types of error indicators related to the discretization and linearization of the problem were established. Furthermore, the first contribution to deriving an *a posteriori* error analysis of the primal-mixed finite element method for the Navier–Stokes/Darcy–Forchheimer coupled problem was proposed and analyzed in [9]. Specifically, [9] extended the usual techniques employed within the Hilbertian framework to Banach spaces by deriving a reliable and efficient *a posteriori* error estimator for the mixed finite element method introduced in [5]. This work includes corresponding local estimates and new Helmholtz decompositions for reliability, as well as inverse inequalities and local estimates of bubble functions for efficiency. Meanwhile, [6] presents the first *a posteriori* error analysis for an augmented mixed finite element method applied to the stationary CBF equations within a Hilbert framework. Additionally, [3] is noted for its *a posteriori* error analysis of a momentum-conservative Banach space-based mixed finite element method for the Navier–Stokes problem. In this work, standard arguments based on duality techniques, a suitable Helmholtz decomposition in Banach frameworks, and classical approximation properties are combined with corresponding small data assumptions to establish the reliability of the estimators. Similar techniques are applied in [13] and [22] to develop reliable and efficient residual-based *a posteriori* error estimators in 2D and 3D for non-augmented Banach spaces-based mixed finite element methods for the stationary Boussinesq and Oberbeck-Boussinesq systems. Finally, we refer to [10] and [8] for recent *a posteriori* error analyses of partially augmented and Banach spaces-based mixed formulations for the coupled Brinkman–Forchheimer and double-diffusion equations.

According to the above discussion, and to complement the study started in [7] for the CBF equations, in the present paper we employ and adapt the *a posteriori* error analysis techniques developed in [9], [3], [13], and [22] for Banach spaces-based mixed formulations to the current CBF model. We develop a reliable and efficient residual-based *a posteriori* error estimator in 2D and 3D for the mixed finite element method from [7]. More precisely, we derive a global quantity Θ that is expressed in terms of calculable local indicators Θ_T defined on each element T of a given triangulation $\mathcal{T}$. This information can then be used to localize sources of error and construct an algorithm to efficiently adapt the mesh. In this way, the estimator Θ is said to be efficient (resp. reliable) if there exists a positive constant

$C_{\mathtt{eff}}$ (resp. $C_{\mathtt{rel}}$), independent of the mesh sizes, such that

$$C_{\mathtt{eff}}\,\Theta \,+\, \mathtt{h.o.t.} \;\leq\; \|\mathrm{error}\| \;\leq\; C_{\mathtt{rel}}\,\Theta \,+\, \mathtt{h.o.t.}\,,$$

where `h.o.t.` is a generic expression denoting one or several terms of higher order. We remark that up to the authors' knowledge, the present work provides the first *a posteriori* error analyses of non-augmented Banach spaces-based mixed finite element methods for the stationary CBF equations.

This paper is organized as follows. The remainder of this section introduces some standard notations and functional spaces. In Section 2, we recall from [7] the model problem and its continuous and discrete mixed variational formulations. Next, in Section 3, we derive in full detail a reliable and efficient residual-based *a posteriori* error estimator for both 2D and 3D settings. Several numerical results illustrating the reliability and efficiency of the *a posteriori* error estimator, as well as the good performance of the associated adaptive algorithm and the recovery of optimal rates of convergence, are reported in Section 4. Finally, further properties to be utilized for the derivation of the reliability and efficiency estimates are provided in Appendices A and B, respectively.

1.1 Preliminary notations

Let $\Omega \subset \mathrm{R}^d, d \in \{2,3\}$, be a bounded domain with polyhedral boundary Γ, and let $\mathbf{n}$ be the outward unit normal vector on Γ. Standard notation will be adopted for Lebesgue spaces $\mathrm{L}^p(\Omega)$ and Sobolev spaces $\mathrm{W}^{s,p}(\Omega)$, with $s \in \mathrm{R}$ and $p > 1$, whose corresponding norms, either for the scalar, vectorial, or tensorial case, are written as $\|\cdot\|_{0,p;\Omega}$ and $\|\cdot\|_{s,p;\Omega}$, respectively. In addition, given a non-negative integer m, $\mathrm{W}^{m,2}(\Omega)$ is also denoted by $\mathrm{H}^m(\Omega)$, and the notations of its norm and seminorm are simplified to $\|\cdot\|_{m,\Omega}$ and $|\cdot|_{m,\Omega}$, respectively. By $\mathbf{M}$ and $\mathbb{M}$ we mean the corresponding vectorial and tensorial counterparts of the generic scalar functional space M, whereas M' represents its dual space, whose norm is defined by $\|f\|_{\mathrm{M}'} := \sup_{0\neq v\in \mathrm{M}} \dfrac{|f(v)|}{\|v\|_{\mathrm{M}}}$. In particular, we set $\mathbf{R} := \mathrm{R}^d$ and $\mathbb{R} := \mathrm{R}^{d\times d}$. In turn, for any vector fields $\mathbf{v} = (v_i)_{i=1,d}$ and $\mathbf{w} = (w_i)_{i=1,d}$, we define the gradient, divergence, and tensor product operators, as $\nabla\mathbf{v} := \left(\dfrac{\partial v_i}{\partial x_j}\right)_{i,j=1,d}$, $\mathrm{div}(\mathbf{v}) := \displaystyle\sum_{j=1}^{d} \frac{\partial v_j}{\partial x_j}$, and $\mathbf{v}\otimes\mathbf{w} := (v_i w_j)_{i,j=1,d}$. Also, for any tensor fields $\boldsymbol{\tau} = (\tau_{ij})_{i,j=1,d}$ and $\boldsymbol{\zeta} = (\zeta_{ij})_{i,j=1,d}$, we let $\mathbf{div}(\boldsymbol{\tau})$ be the usual divergence operator div acting along the rows of $\boldsymbol{\tau}$, and define the transpose, the trace, the tensor inner product, and the deviatoric tensor, respectively, as $\boldsymbol{\tau}^{\mathrm{t}} := (\tau_{ji})_{i,j=1,d}$, $\mathrm{tr}(\boldsymbol{\tau}) := \displaystyle\sum_{i=1}^{d} \tau_{ii}$, $\boldsymbol{\tau} : \boldsymbol{\zeta} := \displaystyle\sum_{i,j=1}^{d} \tau_{ij}\,\zeta_{ij}$, and $\boldsymbol{\tau}^{\mathrm{d}} := \boldsymbol{\tau} - \dfrac{1}{d}\,\mathrm{tr}(\boldsymbol{\tau})\,\mathbb{I}$, where $\mathbb{I}$ is the identity matrix in $\mathbb{R}$. In what follows, when no confusion arises, $|\cdot|$ denotes the Euclidean norm in $\mathbf{R}$ or $\mathbb{R}$. Furthermore, $\mathbf{H}^{1/2}(\Gamma)$ is the space of traces of functions of $\mathbf{H}^1(\Omega)$ and $\mathbf{H}^{-1/2}(\Gamma)$ is its dual, whereas $\langle\cdot,\cdot\rangle_\Gamma$ stands for the corresponding product of duality between $\mathbf{H}^{-1/2}(\Gamma)$ and $\mathbf{H}^{1/2}(\Gamma)$.

2 The model problem and its mixed variational formulation

In this section we recall from [7] the model problem, its mixed variational formulation, the associated Galerkin scheme, and the main results concerning the corresponding solvability analysis.

2.1 The stationary convective Brinkman–Forchheimer equations

In what follows we consider the model analyzed in [7] (see also [14, 32, 28, 31, 6]), which is given by the stationary convective Brinkman–Forchheimer equations. More precisely, given a body force $\mathbf{f}$, we focus on finding a velocity field $\mathbf{u}$, and a pressure field p, such that

$$\begin{array}{rcll} -\nu\,\Delta\mathbf{u} + (\nabla\mathbf{u})\mathbf{u} + \mathtt{D}\,\mathbf{u} + \mathtt{F}\,|\mathbf{u}|^{\rho-2}\mathbf{u} + \nabla p &=& \mathbf{f} & \text{in} \quad \Omega\,, \\ \mathrm{div}(\mathbf{u}) &=& 0 & \text{in} \quad \Omega\,, \\ \mathbf{u} &=& \mathbf{u}_{\mathrm{D}} & \text{on} \quad \Gamma\,, \\ \displaystyle\int_\Omega p &=& 0\,, & \end{array} \tag{2.1}$$

where $\nu > 0$ is the Brinkman coefficient (or the effective viscosity), $\mathtt{D} > 0$ is the Darcy coefficient, $\mathtt{F} > 0$ is the Forchheimer coefficient, and ρ is a given number in $[3, 4]$. Owing to the incompressibility of the fluid, the datum $\mathbf{u}_{\mathrm{D}} \in \mathbf{H}^{1/2}(\Gamma)$ must satisfy the compatibility condition

$$\int_\Gamma \mathbf{u}_{\mathrm{D}} \cdot \mathbf{n} \,=\, 0\,. \tag{2.2}$$

Next, in order to derive a mixed formulation for (2.1), in which the Dirichlet boundary condition for the velocity becomes a natural one, we now proceed as in [4] (see similar approaches in [12, 2, 6]), and introduce as a further unknown the nonlinear pseudostress tensor $\boldsymbol{\sigma}$, which is defined by

$$\boldsymbol{\sigma} := \nu\,\nabla\mathbf{u} - (\mathbf{u}\otimes\mathbf{u}) - p\,\mathbb{I}\,. \tag{2.3}$$

In this way, applying the matrix trace to the tensor $\boldsymbol{\sigma}$, and utilizing the incompressibility condition $\mathrm{div}(\mathbf{u}) = 0$ in Ω, one arrives at

$$p = -\frac{1}{d}\,\mathrm{tr}(\boldsymbol{\sigma} + \mathbf{u}\otimes\mathbf{u})\,. \tag{2.4}$$

Hence, replacing back (2.4) into (2.3), we find that (2.1) can be rewritten, equivalently, as follows: Find $(\boldsymbol{\sigma}, \mathbf{u})$ in suitable spaces to be indicated below such that

$$\begin{array}{rcll} \dfrac{1}{\nu}\,\boldsymbol{\sigma}^{\mathrm{d}} + \dfrac{1}{\nu}\,(\mathbf{u}\otimes\mathbf{u})^{\mathrm{d}} &=& \nabla\mathbf{u} & \text{in} \quad \Omega\,, \\ \mathtt{D}\,\mathbf{u} + \mathtt{F}\,|\mathbf{u}|^{\rho-2}\mathbf{u} - \mathbf{div}(\boldsymbol{\sigma}) &=& \mathbf{f} & \text{in} \quad \Omega\,, \\ \mathbf{u} &=& \mathbf{u}_{\mathrm{D}} & \text{on} \quad \Gamma\,, \\ \displaystyle\int_\Omega \mathrm{tr}(\boldsymbol{\sigma} + \mathbf{u}\otimes\mathbf{u}) &=& 0\,. & \end{array} \tag{2.5}$$

Note that (2.4) and the last equation of (2.5) establish that $\int_\Omega p = 0$, which is required for purposes of uniqueness of the pressure.

2.2 The mixed variational formulation

We first recall from [7, Section 2.2] the following tensorial functional space

$$\mathbb{H}(\mathbf{div}_{4/3};\Omega) \,:=\, \Big\{ \boldsymbol{\tau} \in \mathbb{L}^2(\Omega) \,:\quad \mathbf{div}(\boldsymbol{\tau}) \in \mathbf{L}^{4/3}(\Omega) \Big\}\,,$$

endowed with the norm $\|\boldsymbol{\tau}\|_{\mathbf{div}_{4/3};\Omega} := \|\boldsymbol{\tau}\|_{0,\Omega} + \|\mathbf{div}(\boldsymbol{\tau})\|_{0,4/3;\Omega}$, and observe that the following decomposition holds:

$$\mathbb{H}(\mathbf{div}_{4/3};\Omega) \,=\, \mathbb{H}_0(\mathbf{div}_{4/3};\Omega) \oplus \mathrm{R}\,\mathbb{I}\,, \tag{2.6}$$

where

$$\mathbb{H}_0(\mathbf{div}_{4/3};\Omega) := \left\{ \boldsymbol{\tau} \in \mathbb{H}(\mathbf{div}_{4/3};\Omega) : \quad \int_\Omega \mathrm{tr}(\boldsymbol{\tau}) = 0 \right\}.$$

Hence, proceeding as in [7, eq. (2.14)], that is, multiplying the first two equations in (2.5) by suitable test functions, integrating by parts, using (2.2) and the Dirichlet boundary condition, we find that the mixed variational formulation of (2.5) reduces to: Find $(\boldsymbol{\sigma}, \mathbf{u}) \in \mathbb{H}_0(\mathbf{div}_{4/3};\Omega) \times \mathbf{L}^4(\Omega)$ such that

$$\begin{aligned} a(\boldsymbol{\sigma},\boldsymbol{\tau}) + b(\boldsymbol{\tau},\mathbf{u}) + \frac{1}{\nu}\int_\Omega (\mathbf{u}\otimes\mathbf{u})^{\mathrm{d}} : \boldsymbol{\tau} &= \langle \boldsymbol{\tau}\mathbf{n}, \mathbf{u}_{\mathrm{D}} \rangle_\Gamma \quad \forall\, \boldsymbol{\tau} \in \mathbb{H}_0(\mathbf{div}_{4/3};\Omega)\,, \\ b(\boldsymbol{\sigma},\mathbf{v}) - c(\mathbf{u},\mathbf{v}) - \mathtt{F}\int_\Omega |\mathbf{u}|^{\rho-2}\mathbf{u}\cdot\mathbf{v} &= -\int_\Omega \mathbf{f}\cdot\mathbf{v} \quad \forall\, \mathbf{v} \in \mathbf{L}^4(\Omega)\,, \end{aligned} \tag{2.7}$$

where, the bilinear forms $a : \mathbb{H}_0(\mathbf{div}_{4/3};\Omega) \times \mathbb{H}_0(\mathbf{div}_{4/3};\Omega) \to \mathrm{R}$, $b : \mathbb{H}_0(\mathbf{div}_{4/3};\Omega) \times \mathbf{L}^4(\Omega) \to \mathrm{R}$, and $c : \mathbf{L}^4(\Omega) \times \mathbf{L}^4(\Omega) \to \mathrm{R}$, are defined as

$$a(\boldsymbol{\zeta},\boldsymbol{\tau}) := \frac{1}{\nu}\int_\Omega \boldsymbol{\zeta}^{\mathrm{d}} : \boldsymbol{\tau}^{\mathrm{d}}\,, \quad b(\boldsymbol{\tau},\mathbf{v}) := \int_\Omega \mathbf{v}\cdot\mathbf{div}(\boldsymbol{\tau})\,, \quad \text{and} \quad c(\mathbf{z},\mathbf{v}) := \mathtt{D}\int_\Omega \mathbf{z}\cdot\mathbf{v}\,, \tag{2.8}$$

for all $(\boldsymbol{\zeta},\mathbf{z}), (\boldsymbol{\tau},\mathbf{v}) \in \mathbb{H}_0(\mathbf{div}_{4/3};\Omega) \times \mathbf{L}^4(\Omega)$. Equivalently, defining the space $\mathbf{X} := \mathbb{H}_0(\mathbf{div}_{4/3};\Omega) \times \mathbf{L}^4(\Omega)$ equipped with the product norm

$$\|(\boldsymbol{\tau},\mathbf{v})\|_{\mathbf{X}} := \|\boldsymbol{\tau}\|_{\mathbf{div}_{4/3};\Omega} + \|\mathbf{v}\|_{0,4;\Omega} \quad \forall\, (\boldsymbol{\tau},\mathbf{v}) \in \mathbf{X}\,,$$

and introducing, for each $\mathbf{w} \in \mathbf{L}^4(\Omega)$, the bilinear form $\mathbf{A}_{\mathbf{w}} : \mathbf{X}\times\mathbf{X} \to \mathrm{R}$ defined by

$$\mathbf{A}_{\mathbf{w}}((\boldsymbol{\zeta},\mathbf{z}),(\boldsymbol{\tau},\mathbf{v})) := \mathbf{A}((\boldsymbol{\zeta},\mathbf{z}),(\boldsymbol{\tau},\mathbf{v})) + \mathbf{B}_{\mathbf{w}}((\boldsymbol{\zeta},\mathbf{z}),(\boldsymbol{\tau},\mathbf{v}))\,, \tag{2.9}$$

with

$$\mathbf{A}((\boldsymbol{\zeta},\mathbf{z}),(\boldsymbol{\tau},\mathbf{v})) := a(\boldsymbol{\zeta},\boldsymbol{\tau}) + b(\boldsymbol{\tau},\mathbf{z}) + b(\boldsymbol{\zeta},\mathbf{v}) - c(\mathbf{z},\mathbf{v})\,, \quad \text{and} \tag{2.10}$$

$$\mathbf{B}_{\mathbf{w}}((\boldsymbol{\zeta},\mathbf{z}),(\boldsymbol{\tau},\mathbf{v})) := \frac{1}{\nu}\int_\Omega (\mathbf{w}\otimes\mathbf{z})^{\mathrm{d}} : \boldsymbol{\tau} - \mathtt{F}\int_\Omega |\mathbf{w}|^{\rho-2}\mathbf{z}\cdot\mathbf{v}\,, \tag{2.11}$$

for all $(\boldsymbol{\zeta},\mathbf{z}), (\boldsymbol{\tau},\mathbf{v}) \in \mathbf{X}$, we deduce that (2.7) can be re-stated as (cf. [7, eq. (2.19)]): Find $(\boldsymbol{\sigma},\mathbf{u}) \in \mathbf{X}$ such that

$$\mathbf{A}_{\mathbf{u}}((\boldsymbol{\sigma},\mathbf{u}),(\boldsymbol{\tau},\mathbf{v})) = \mathbf{F}(\boldsymbol{\tau},\mathbf{v}) \quad \forall\, (\boldsymbol{\tau},\mathbf{v}) \in \mathbf{X}\,, \tag{2.12}$$

where $\mathbf{F} \in \mathbf{X}'$ is defined by

$$\mathbf{F}(\boldsymbol{\tau},\mathbf{v}) := \langle \boldsymbol{\tau}\mathbf{n}, \mathbf{u}_{\mathrm{D}} \rangle_\Gamma - \int_\Omega \mathbf{f}\cdot\mathbf{v} \quad \forall\, (\boldsymbol{\tau},\mathbf{v}) \in \mathbf{X}\,. \tag{2.13}$$

The well-posednees of (2.12) (equivalently of (2.7)), which makes use of a fixed-point estrategy along with a recent result for perturbed saddle-point formulations in Banach spaces (cf. [16, Theorem 3.4]) and the Banach–Nečas–Babuška theorem, is established by [7, Theorem 1]. More precisely, given $r \in (0, r_0]$, with $r_0 := \min\{r_1, r_2\}$ and

$$r_1 := \frac{\nu\,\gamma}{4} \quad \text{and} \quad r_2 := \left(\frac{\gamma}{4\,\mathtt{F}\,|\Omega|^{(4-\rho)/4}} \right)^{1/(\rho-2)}\,, \tag{2.14}$$

with γ the positive constant, independent of h, establishing a global inf-sup condition of the bilinear form $\mathbf{A}$ (cf. (2.10) and [7, eq. (3.10)]), and under a smallness assumptions on the data, namely

those detailed in [7, eqs. (3.18) and (3.26)], it is proved that a suitable operator mapping the ball $\mathbf{W}_r := \Big\{ \mathbf{w} \in \mathbf{L}^4(\Omega) : \quad \|\mathbf{w}\|_{0,4;\Omega} \leq r \Big\}$ into itself, has a unique fixed-point $\mathbf{u}$ in it, which yields the unique solution $(\boldsymbol{\sigma}, \mathbf{u}) \in \mathbf{X}$ of (2.12), with $\mathbf{u} \in \mathbf{W}_r$. In addition, according to [7, eq. (3.16)] and using the fact that $\mathbf{u} \in \mathbf{W}_r$, we observe that the bilinear form $\mathbf{A}_{\mathbf{u}}$ (cf. (2.9)) satisfies the following global inf-sup condition

$$\sup_{\mathbf{0} \neq (\boldsymbol{\tau}, \mathbf{v}) \in \mathbf{X}} \frac{\mathbf{A}_{\mathbf{u}}((\boldsymbol{\zeta}, \mathbf{z}), (\boldsymbol{\tau}, \mathbf{v}))}{\|(\boldsymbol{\tau}, \mathbf{v})\|_{\mathbf{X}}} \geq \frac{\gamma}{2} \|(\boldsymbol{\zeta}, \mathbf{z})\|_{\mathbf{X}} \quad \forall\, (\boldsymbol{\zeta}, \mathbf{z}) \in \mathbf{X}\,. \tag{2.15}$$

2.3 The Galerkin scheme

We denote by $h := \max\big\{h_T : \ T \in \mathcal{T}_h\big\}$ the size of a regular triangulation $\mathcal{T}_h$ of $\overline{\Omega}$ made up of triangles T (when $d = 2$) or tetrahedra T (when $d = 3$) of diameter h_T. In addition, given an integer $\ell \geq 0$ and a subset S of $\mathbf{R}$, we denote by $\mathrm{P}_\ell(S)$ the space of polynomials of total degree at most ℓ defined on S. Hence, for each integer $k \geq 0$ and for each $T \in \mathcal{T}_h$, we define the local Raviart–Thomas space of order k as

$$\mathbf{RT}_k(T) := \mathbf{P}_k(T) \oplus \widetilde{\mathrm{P}}_k(T)\,\mathbf{x}\,,$$

where $\mathbf{x} := (x_1, \ldots, x_d)^{\mathrm{t}}$ is a generic vector of $\mathbf{R}$, $\widetilde{\mathrm{P}}_k(T)$ is the space of polynomials of total degree equal to k defined on T, and, according to the convention in Section 1, we set $\mathbf{P}_k(T) := [\mathrm{P}_k(T)]^d$. Then, denoting by $\boldsymbol{\tau}_{h,i}$ the i-th row of a tensor $\boldsymbol{\tau}_h$, we recall from [7, Section 4.3] the finite element subspaces on Ω:

$$\widetilde{\mathbb{H}}_h^{\boldsymbol{\sigma}} := \Big\{ \boldsymbol{\tau}_h \in \mathbb{H}(\mathbf{div}_{4/3}; \Omega) : \quad \boldsymbol{\tau}_{h,i}|_T \in \mathbf{RT}_k(T) \quad \forall\, i \in \big\{1, \ldots, d\big\}\,, \quad \forall\, T \in \mathcal{T}_h \Big\}\,,$$

$$\mathbf{H}_h^{\mathbf{u}} := \Big\{ \mathbf{v}_h \in \mathbf{L}^4(\Omega) : \quad \mathbf{v}_h|_T \in \mathbf{P}_k(T) \quad \forall\, T \in \mathcal{T}_h \Big\}\,.$$

Thus, letting

$$\mathbb{H}_h^{\boldsymbol{\sigma}} := \widetilde{\mathbb{H}}_h^{\boldsymbol{\sigma}} \cap \mathbb{H}_0(\mathbf{div}_{4/3}; \Omega)\,,$$

the Galerkin scheme associated with (2.7) reads: Find $(\boldsymbol{\sigma}_h, \mathbf{u}_h) \in \mathbb{H}_h^{\boldsymbol{\sigma}} \times \mathbf{H}_h^{\mathbf{u}}$ such that

$$\begin{aligned} a(\boldsymbol{\sigma}_h, \boldsymbol{\tau}_h) + b(\boldsymbol{\tau}_h, \mathbf{u}_h) + \frac{1}{\nu} \int_\Omega (\mathbf{u}_h \otimes \mathbf{u}_h)^{\mathrm{d}} : \boldsymbol{\tau}_h &= \langle \boldsymbol{\tau}_h \mathbf{n}, \mathbf{u}_{\mathrm{D}} \rangle_\Gamma \quad \forall\, \boldsymbol{\tau}_h \in \mathbb{H}_h^{\boldsymbol{\sigma}}\,, \\ b(\boldsymbol{\sigma}_h, \mathbf{v}_h) - c(\mathbf{u}_h, \mathbf{v}_h) - \mathtt{F} \int_\Omega |\mathbf{u}_h|^{\rho-2} \mathbf{u}_h \cdot \mathbf{v}_h &= -\int_\Omega \mathbf{f} \cdot \mathbf{v}_h \quad \forall\, \mathbf{v}_h \in \mathbf{H}_h^{\mathbf{u}}\,. \end{aligned} \tag{2.16}$$

Similarly, setting $\mathbf{X}_h := \mathbb{H}_h^{\boldsymbol{\sigma}} \times \mathbf{H}_h^{\mathbf{u}}$, the Galerkin scheme associated with (2.12), which is certainly equivalent to (2.16), becomes: Find $(\boldsymbol{\sigma}_h, \mathbf{u}_h) \in \mathbf{X}_h$ such that

$$\mathbf{A}_{\mathbf{u}_h}((\boldsymbol{\sigma}_h, \mathbf{u}_h), (\boldsymbol{\tau}_h, \mathbf{v}_h)) = \mathbf{F}(\boldsymbol{\tau}_h, \mathbf{v}_h) \quad \forall\, (\boldsymbol{\tau}_h, \mathbf{v}_h) \in \mathbf{X}_h\,. \tag{2.17}$$

The solvability analysis and *a priori* error bounds for (2.17) (equivalently of (2.16)) are established in [7, Theorems 2 and 4], respectively. Indeed, similarly as remarked at the end of Section 2.2, and under the discrete analogues of the assumptions [7, eqs. (3.18) and (3.26)], which are detailed in [7, eqs. (4.13) and (4.15)], given $\widetilde{r} \in (0, \widetilde{r}_0]$, with $\widetilde{r}_0 := \min\{\widetilde{r}_1, \widetilde{r}_2\}$ and

$$\widetilde{r}_1 := \frac{\nu\, \gamma_{\mathtt{d}}}{4} \quad \text{and} \quad \widetilde{r}_2 := \left(\frac{\gamma_{\mathtt{d}}}{4\, \mathtt{F}\, |\Omega|^{(4-\rho)/4}} \right)^{1/(\rho-2)}\,, \tag{2.18}$$

with $\gamma_{\mathtt{d}}$ the positive constant, independent of h, establishing a global discrete inf-sup condition for the bilinear form $\mathbf{A}$ (cf. (2.10) and [7, eq. (4.8)]), it is proved that a suitable discrete operator mapping

the ball $\mathbf{W}_{\widetilde{r}} := \left\{ \mathbf{w}_h \in \mathbf{H}_h^{\mathbf{u}} : \quad \|\mathbf{w}_h\|_{0,4;\Omega} \leq \widetilde{r} \right\}$ into itself, has a unique fixed-point $\mathbf{u}_h$ in it, which yields the unique $(\boldsymbol{\sigma}_h, \mathbf{u}_h) \in \mathbf{X}_h$ of (2.17), with $\mathbf{u}_h \in \mathbf{W}_{\widetilde{r}}$. In particular, we recall for later use the following *a priori* estimate

$$\|(\boldsymbol{\sigma}_h, \mathbf{u}_h)\|_{\mathbf{X}} \leq \frac{2\, C_{\mathbf{F}}}{\gamma_{\mathtt{d}}} \left\{ \|\mathbf{f}\|_{0,4/3;\Omega} + \|\mathbf{u}_{\mathrm{D}}\|_{1/2,\Gamma} \right\}, \tag{2.19}$$

where $C_{\mathbf{F}} := \max\{1, \|\mathbf{i}_4\|\}$ and $\|\mathbf{i}_4\|$ is the norm of the continuous injection $\mathbf{i}_4$ of $\mathbf{H}^1(\Omega)$ into $\mathbf{L}^4(\Omega)$ (cf. (2.13) and [7, eq. (3.4)]).

3 *A posteriori* error analysis

In this section we derive a reliable an efficient residual based *a posteriori* error estimator for the Galerkin scheme (2.16) (equivalently (2.17)). To this end, from now on we employ the notations and results from Appendix A. Recalling that $(\boldsymbol{\sigma}_h, \mathbf{u}_h) \in \mathbf{X}_h$ is the unique solution of the discrete problem (2.17), we define the global *a posteriori* error estimator Θ by

$$\Theta := \left\{ \sum_{T \in \mathcal{T}_h} \Theta_{1,T}^4 \right\}^{1/4} + \left\{ \sum_{T \in \mathcal{T}_h} \Theta_{2,T}^2 \right\}^{1/2} + \left\{ \sum_{T \in \mathcal{T}_h} \Theta_{3,T}^{4/3} \right\}^{3/4}, \tag{3.1}$$

where, for each $T \in \mathcal{T}_h$, the local error indicators $\Theta_{1,T}^4$, $\Theta_{2,T}^2$, and $\Theta_{3,T}^{4/3}$ are defined as

$$\Theta_{1,T}^4 := h_T^4 \left\| \nabla \mathbf{u}_h - \frac{1}{\nu} \big(\boldsymbol{\sigma}_h + (\mathbf{u}_h \otimes \mathbf{u}_h) \big)^{\mathrm{d}} \right\|_{0,4;T}^4 + \sum_{e \in \mathcal{E}_{h,T}(\Gamma)} h_e \, \|\mathbf{u}_{\mathrm{D}} - \mathbf{u}_h\|_{0,4;e}^4 , \tag{3.2}$$

$$\begin{aligned} \Theta_{2,T}^2 := {} & h_T^2 \left\| \underline{\mathbf{curl}} \left(\frac{1}{\nu} \big(\boldsymbol{\sigma}_h + (\mathbf{u}_h \otimes \mathbf{u}_h) \big)^{\mathrm{d}} \right) \right\|_{0,T}^2 \\ & + \sum_{e \in \mathcal{E}_{h,T}(\Omega)} h_e \left\| \left[\!\left[\boldsymbol{\delta}_* \left(\frac{1}{\nu} \big(\boldsymbol{\sigma}_h + (\mathbf{u}_h \otimes \mathbf{u}_h) \big)^{\mathrm{d}} \right) \right]\!\right] \right\|_{0,e}^2 \\ & + \sum_{e \in \mathcal{E}_{h,T}(\Gamma)} h_e \left\| \boldsymbol{\delta}_* \left(\nabla \mathbf{u}_{\mathrm{D}} - \frac{1}{\nu} \big(\boldsymbol{\sigma}_h + (\mathbf{u}_h \otimes \mathbf{u}_h) \big)^{\mathrm{d}} \right) \right\|_{0,e}^2 , \end{aligned} \tag{3.3}$$

and

$$\Theta_{3,T}^{4/3} := \left\| \mathbf{f} + \mathbf{div}(\boldsymbol{\sigma}_h) - \mathtt{D}\, \mathbf{u}_h - \mathtt{F}\, |\mathbf{u}_h|^{\rho-2} \mathbf{u}_h \right\|_{0,4/3;T}^{4/3} , \tag{3.4}$$

where the jump and tangential component operators $[\![\,]\!]$ and $\boldsymbol{\delta}_*$ are defined in (A.1) and (A.2), respectively. Notice that the last term of $\Theta_{2,T}^2$ requires $\boldsymbol{\delta}_*(\nabla \mathbf{u}_{\mathrm{D}})|_e \in \mathbf{L}^2(e)$ for all $e \in \mathcal{E}_h(\Gamma)$, which is guaranteed below by simply assuming that $\mathbf{u}_{\mathrm{D}} \in \mathbf{H}^1(\Gamma)$. Nevertheless, aiming to be more precise, one just needs that $\nabla \mathbf{u}_{\mathrm{D}}|_\Gamma \in \mathbb{L}^2(\Gamma)$ for which it would actually suffice to assume that $\nabla \mathbf{u}_{\mathrm{D}}|_\Gamma$ coincides with the trace of the gradient of a function in $\mathbf{H}^t(\Omega)$, for some $t > 3/2$. In any case, we stress that the Dirichlet data of the numerical results reported below in Section 4 do verify the firstly mentioned assumption on $\mathbf{u}_{\mathrm{D}}$.

The main goal of the present section is to establish, under suitable assumptions, the existence of positive constants $C_{\mathtt{eff}}$ and $C_{\mathtt{rel}}$, independent of the meshsizes and the continuous and discrete solutions, such that

$$C_{\mathtt{eff}}\, \Theta + \mathtt{h.o.t} \leq \|(\boldsymbol{\sigma}, \mathbf{u}) - (\boldsymbol{\sigma}_h, \mathbf{u}_h)\|_{\mathbf{X}} \leq C_{\mathtt{rel}}\, \Theta , \tag{3.5}$$

where h.o.t. is a generic expression denoting one or several terms of higher order. The upper and lower bounds in (3.5), which are known as the reliability and efficiency of Θ, are derived below in Sections 3.1 and 3.2, respectively.

3.1 Reliability of the *a posteriori* error estimator

The main result of this section is stated in the following theorem. To this end, we first let

$$\overline{r}_0 := \min\{r_1, r_2, \widetilde{r}_2\} \quad \text{and} \quad \widehat{\gamma} := \min\{\gamma, \gamma_{\mathtt{d}}\}\,, \tag{3.6}$$

where, r_1, r_2 and $\widetilde{r}_2$ are defined in (2.14) and (2.18), respectively, whereas $\widehat{\gamma}$ is the same constant in [7, eq. (5.1)] employed to derive the *a priori* error estimate stated in [7, Theorem 3]. In addition, we recall from [25, Lemma 5.3] that for each $m \geq 2$ there exists a constant $C(m) > 0$ such that

$$\big||\mathbf{z}|^{m-2}\mathbf{z} - |\mathbf{y}|^{m-2}\mathbf{y}\big| \,\leq\, C(m)\,\big(|\mathbf{z}| + |\mathbf{y}|\big)^{m-2}|\mathbf{z} - \mathbf{y}| \quad \forall\, \mathbf{z},\, \mathbf{y} \,\in\, \mathbf{R}\,. \tag{3.7}$$

Then, given arbitrary $\mathbf{w}_1$, $\mathbf{w}_2 \in \mathbf{L}^4(\Omega)$, we apply (3.7) to the setting $m = \rho - 1 \in [2,3]$, $\mathbf{z} = (|\mathbf{w}_1|, \mathbf{0})$, and $\mathbf{y} = (|\mathbf{w}_2|, \mathbf{0})$, with $\mathbf{0} \in \mathrm{R}^{d-1}$, denote $c_\rho := C(\rho - 1)$, and conclude that there holds

$$\begin{aligned} \big||\mathbf{w}_1|^{\rho-2} - |\mathbf{w}_2|^{\rho-2}\big| \,&=\, \big||\mathbf{w}_1|^{\rho-3}(|\mathbf{w}_1|, \mathbf{0}) - |\mathbf{w}_2|^{\rho-3}(|\mathbf{w}_2|, \mathbf{0})\big| \\ &\leq\, c_\rho\,\big(|\mathbf{w}_1| + |\mathbf{w}_2|\big)^{\rho-3}\,|\mathbf{w}_1 - \mathbf{w}_2|\,. \end{aligned} \tag{3.8}$$

The aforementioned result is stated now.

Theorem 3.1 *Assume that the data* $\mathbf{f}$ *and* $\mathbf{u}_{\mathrm{D}}$ *satisfy*

$$(1 + 2\,c_\rho)\,\frac{C_{\mathbf{F}}}{\widehat{\gamma}\,\overline{r}_0}\,\Big\{\|\mathbf{f}\|_{0,4/3;\Omega} + \|\mathbf{u}_{\mathrm{D}}\|_{1/2,\Gamma}\Big\} \leq \frac{1}{2}\,. \tag{3.9}$$

Then, there exists a constant $C_{\mathtt{rel}} > 0$*, independent of* h*, such that*

$$\|(\boldsymbol{\sigma}, \mathbf{u}) - (\boldsymbol{\sigma}_h, \mathbf{u}_h)\|_{\mathbf{X}} \,\leq\, C_{\mathtt{rel}}\,\Theta\,. \tag{3.10}$$

We begin the proof of Theorem 3.1 with a preliminary lemma.

Lemma 3.2 *Assume that the data* $\mathbf{f}$ *and* $\mathbf{u}_{\mathrm{D}}$ *satisfy* (3.9)*. Then, there exists a positive constant* C*, independent of* h*, such that*

$$\|(\boldsymbol{\sigma}, \mathbf{u}) - (\boldsymbol{\sigma}_h, \mathbf{u}_h)\|_{\mathbf{X}} \,\leq\, C \sup_{\mathbf{0} \neq (\boldsymbol{\tau}, \mathbf{v}) \in \mathbf{X}} \frac{|\mathcal{R}(\boldsymbol{\tau}, \mathbf{v})|}{\|(\boldsymbol{\tau}, \mathbf{v})\|_{\mathbf{X}}}\,, \tag{3.11}$$

where $\mathcal{R} : \mathbf{X} \to \mathrm{R}$ *is the residual functional given by*

$$\mathcal{R}(\boldsymbol{\tau}, \mathbf{v}) \,:=\, \mathbf{F}(\boldsymbol{\tau}, \mathbf{v}) - \mathbf{A}_{\mathbf{u}_h}((\boldsymbol{\sigma}_h, \mathbf{u}_h), (\boldsymbol{\tau}, \mathbf{v})) \quad \forall\,(\boldsymbol{\tau}, \mathbf{v}) \in \mathbf{X}\,. \tag{3.12}$$

Proof. First, applying the inf-sup condition (2.15) to the error $(\boldsymbol{\zeta}, \mathbf{z}) = (\boldsymbol{\sigma} - \boldsymbol{\sigma}_h, \mathbf{u} - \mathbf{u}_h)$, adding and substracting $\mathbf{B}_{\mathbf{u}_h}((\boldsymbol{\sigma}_h, \mathbf{u}_h), (\boldsymbol{\tau}, \mathbf{v}))$, and using (2.12), we deduce that

$$\frac{\gamma}{2}\,\|(\boldsymbol{\sigma} - \boldsymbol{\sigma}_h, \mathbf{u} - \mathbf{u}_h)\|_{\mathbf{X}} \,\leq\, \sup_{\mathbf{0} \neq (\boldsymbol{\tau}, \mathbf{v}) \in \mathbf{X}} \frac{|\mathcal{R}(\boldsymbol{\tau}, \mathbf{v})|}{\|(\boldsymbol{\tau}, \mathbf{v})\|_{\mathbf{X}}} \,+\, \sup_{\mathbf{0} \neq (\boldsymbol{\tau}, \mathbf{v}) \in \mathbf{X}} \frac{\Big|\big(\mathbf{B}_{\mathbf{u}} - \mathbf{B}_{\mathbf{u}_h}\big)((\boldsymbol{\sigma}_h, \mathbf{u}_h), (\boldsymbol{\tau}, \mathbf{v}))\Big|}{\|(\boldsymbol{\tau}, \mathbf{v})\|_{\mathbf{X}}}\,. \tag{3.13}$$

Then, proceeding similarly as for the derivation of [7, eq. (3.24)], that is, using (3.8) and the continuity bounds [7, eqs. (3.22) and (3.23)], we find that

$$\begin{aligned}\big(\mathbf{B}_{\mathbf{u}}-\mathbf{B}_{\mathbf{u}_h}\big)((\boldsymbol{\sigma}_h,\mathbf{u}_h),(\boldsymbol{\tau},\mathbf{v})) \,&=\, \frac{1}{\nu}\int_\Omega((\mathbf{u}-\mathbf{u}_h)\otimes\mathbf{u}_h)^{\mathrm{d}}:\boldsymbol{\tau}-\mathtt{F}\int_\Omega(|\mathbf{u}|^{\rho-2}-|\mathbf{u}_h|^{\rho-2})\mathbf{u}_h\cdot\mathbf{v}\\ &\leq\left(\frac{1}{\nu}\,+\,\mathtt{F}\,c_\rho\,|\Omega|^{(4-\rho)/4}\big(\|\mathbf{u}\|_{0,4;\Omega}+\|\mathbf{u}_h\|_{0,4;\Omega}\big)^{\rho-3}\right)\|\mathbf{u}-\mathbf{u}_h\|_{0,4;\Omega}\,\|\mathbf{u}_h\|_{0,4;\Omega}\,\|(\boldsymbol{\tau},\mathbf{v})\|_{\mathbf{X}}\,.\end{aligned}\tag{3.14}$$

Next, replacing (3.14) back into (3.13), using the subadditivity inequality for $\rho-3\in[0,1]$, and bounding $\|\mathbf{u}\|_{0,4;\Omega}+\|\mathbf{u}_h\|_{0,4;\Omega}$ by $r_2+\widetilde{r}_2$, which follows from the fact that $\mathbf{u}\in\mathbf{W}_r$ and $\mathbf{u}_h\in\mathbf{W}_{\widetilde{r}}$, with $r\in(0,r_0]$, $r_0:=\min\{r_1,r_2\}$, $\widetilde{r}\in(0,\widetilde{r}_0]$, and $\widetilde{r}_0:=\min\{\widetilde{r}_1,\widetilde{r}_2\}$ (cf. (2.14), (2.18)), we arrive at

$$\begin{aligned}\|(\boldsymbol{\sigma}-\boldsymbol{\sigma}_h,\mathbf{u}-\mathbf{u}_h)\|_{\mathbf{X}}\,&\leq\,\frac{2}{\gamma}\sup_{\mathbf{0}\neq(\boldsymbol{\tau},\mathbf{v})\in\mathbf{X}}\frac{|\mathcal{R}(\boldsymbol{\tau},\mathbf{v})|}{\|(\boldsymbol{\tau},\mathbf{v})\|_{\mathbf{X}}}\\ &+\left(\frac{1}{\gamma_{\mathtt{d}}\,r_1}+\left(\frac{1}{\gamma_{\mathtt{d}}\,r_2}+\frac{1}{\gamma\,\widetilde{r}_2}\right)c_\rho\right)\frac{\gamma_{\mathtt{d}}}{2}\|\mathbf{u}_h\|_{0,4;\Omega}\|\mathbf{u}-\mathbf{u}_h\|_{0,4;\Omega}\,.\end{aligned}$$

Finally, using the fact that $1/r_1,1/r_2,1/\widetilde{r}_2$ and $1/\gamma,1/\gamma_{\mathtt{d}}$ are bounded by $1/\overline{r}_0$ and $1/\widehat{\gamma}$, respectively, with $\overline{r}_0$ and $\widehat{\gamma}$ defined as in (3.6), bounding $\|\mathbf{u}_h\|_{0,4;\Omega}$ as in (2.19), and performing simple algebraic manipulations, we get

$$\begin{aligned}\|(\boldsymbol{\sigma}-\boldsymbol{\sigma}_h,\mathbf{u}-\mathbf{u}_h)\|_{\mathbf{X}}\,&\leq\,\frac{2}{\gamma}\sup_{\mathbf{0}\neq(\boldsymbol{\tau},\mathbf{v})\in\mathbf{X}}\frac{|\mathcal{R}(\boldsymbol{\tau},\mathbf{v})|}{\|(\boldsymbol{\tau},\mathbf{v})\|_{\mathbf{X}}}\\ &+(1+2\,c_\rho)\frac{C_{\mathbf{F}}}{\widehat{\gamma}\,\overline{r}_0}\Big\{\|\mathbf{f}\|_{0,4/3;\Omega}+\|\mathbf{u}_{\mathrm{D}}\|_{1/2,\Gamma}\Big\}\,\|\mathbf{u}-\mathbf{u}_h\|_{0,4;\Omega}\,.\end{aligned}\tag{3.15}$$

Thus, employing (3.9) in (3.15), we obtain (3.11) with $C=4/\gamma$ and end the proof. □

We now aim to bound the supremum in (3.11). Indeed, in virtue of the definitions of the forms $\mathbf{A}_{\mathbf{w}},\mathbf{B}_{\mathbf{w}}$ (cf. (2.8), (2.9), (2.10), (2.11)) and the functionals $\mathbf{F},\mathcal{R}$ (cf. (2.13), (3.12)), we find that, for any $(\boldsymbol{\tau},\mathbf{v})\in\mathbb{H}_0(\mathbf{div}_{4/3};\Omega)\times\mathbf{L}^4(\Omega)$, there holds

$$\mathcal{R}(\boldsymbol{\tau},\mathbf{v})\,=\,\mathcal{R}_1(\boldsymbol{\tau})\,+\,\mathcal{R}_2(\mathbf{v})\,,$$

where

$$\mathcal{R}_1(\boldsymbol{\tau})\,=\,\langle\boldsymbol{\tau}\mathbf{n},\mathbf{u}_{\mathrm{D}}\rangle_\Gamma-\int_\Omega\mathbf{u}_h\cdot\mathbf{div}(\boldsymbol{\tau})-\frac{1}{\nu}\int_\Omega\big(\boldsymbol{\sigma}_h+(\mathbf{u}_h\otimes\mathbf{u}_h)\big)^{\mathrm{d}}:\boldsymbol{\tau}\tag{3.16}$$

and

$$\mathcal{R}_2(\mathbf{v})\,=\,-\int_\Omega\big(\mathbf{f}+\mathbf{div}(\boldsymbol{\sigma}_h)-\mathtt{D}\,\mathbf{u}_h-\mathtt{F}\,|\mathbf{u}_h|^{\rho-2}\mathbf{u}_h\big)\cdot\mathbf{v}\,.\tag{3.17}$$

Then, the supremum in (3.11) can be bounded in terms of $\mathcal{R}_1$ and $\mathcal{R}_2$ as follows

$$\|(\boldsymbol{\sigma}-\boldsymbol{\sigma}_h,\mathbf{u}-\mathbf{u}_h)\|_{\mathbf{X}}\,\leq\,C\Big\{\|\mathcal{R}_1\|_{\mathbb{H}_0(\mathbf{div}_{4/3};\Omega)'}\,+\,\|\mathcal{R}_2\|_{\mathbf{L}^4(\Omega)'}\Big\}\,,\tag{3.18}$$

and hence our next purpose is to derive suitable upper bounds for the two terms on the right-hand side of (3.18). We begin by establishing the corresponding estimate for $\mathcal{R}_2$ (cf. (3.17)), which follow from a straightforward application of the Hölder inequality.

Lemma 3.3 *There holds*

$$\|\mathcal{R}_2\|_{\mathbf{L}^4(\Omega)'}\,\leq\,\left\{\sum_{T\in\mathcal{T}_h}\big\|\mathbf{f}+\mathbf{div}(\boldsymbol{\sigma}_h)-\mathtt{D}\,\mathbf{u}_h-\mathtt{F}\,|\mathbf{u}_h|^{\rho-2}\mathbf{u}_h\big\|^{4/3}_{0,4/3;T}\right\}^{3/4}\quad.$$

We now turn to the derivation of the corresponding estimate for $\|\mathcal{R}_1\|_{\mathbb{H}_0(\mathbf{div}_{4/3};\Omega)'}$. To that end, we first deduce from the definition of $\mathcal{R}_1$ (cf. (3.16)) and the first equation of the Galerkin scheme (2.16) (cf. (2.17)) that $\mathcal{R}_1(\boldsymbol{\tau}_h)=0$ for all $\boldsymbol{\tau}_h\in\mathbb{H}_h^{\boldsymbol{\sigma}}$, whence in the computation of

$$\|\mathcal{R}_1\|_{\mathbb{H}_0(\mathbf{div}_{4/3};\Omega)'} := \sup_{\mathbf{0}\neq\boldsymbol{\tau}\in\mathbb{H}_0(\mathbf{div}_{4/3};\Omega)} \frac{\mathcal{R}_1(\boldsymbol{\tau})}{\|\boldsymbol{\tau}\|_{\mathbf{div}_{4/3};\Omega}}\,, \tag{3.19}$$

we can replace each term $\mathcal{R}_1(\boldsymbol{\tau})$ by $\mathcal{R}_1(\boldsymbol{\tau}-\boldsymbol{\tau}_h)$, with a suitable $\boldsymbol{\tau}_h\in\mathbb{H}_h^{\boldsymbol{\sigma}}$ depending on the given $\boldsymbol{\tau}\in\mathbb{H}_0(\mathbf{div}_{4/3};\Omega)$. Indeed, we first consider the Helmholtz decomposition provided by Lemma A.2 part (b) (respectively (a) for the 2D setting), with $p=4/3$, which says that for each $\boldsymbol{\tau}\in\mathbb{H}_0(\mathbf{div}_{4/3};\Omega)$ there exist $\boldsymbol{\zeta}\in\mathbb{W}^{1,4/3}(\Omega)$ and $\boldsymbol{\xi}\in\mathbb{H}^1(\Omega)$, such that

$$\boldsymbol{\tau} \,=\, \boldsymbol{\zeta}+\underline{\mathbf{curl}}(\boldsymbol{\xi}) \quad \text{in} \quad \Omega \quad \text{and} \quad \|\boldsymbol{\zeta}\|_{1,4/3;\Omega}+\|\boldsymbol{\xi}\|_{1,\Omega} \,\leq\, C_{4/3}\,\|\boldsymbol{\tau}\|_{\mathbf{div}_{4/3};\Omega}\,, \tag{3.20}$$

with a positive constant $C_{4/3}$ independent of $\boldsymbol{\tau}$. Then, setting

$$\boldsymbol{\tau}_h \,:=\, \boldsymbol{\Pi}_h^k(\boldsymbol{\zeta})+\underline{\mathbf{curl}}(\boldsymbol{\mathcal{I}}_h(\boldsymbol{\xi}))+c\,\mathbb{I}\,, \tag{3.21}$$

where $\boldsymbol{\Pi}_h^k$ and $\boldsymbol{\mathcal{I}}_h$ are the tensor versions of the Raviart-Thomas and Clément interpolation operators (cf. Appendix A), respectively, and the constant c is chosen so that $\mathrm{tr}(\boldsymbol{\tau}_h)$ has a null mean value, we readily see that $\boldsymbol{\tau}_h$, which can be seen as a discrete Helmholtz decomposition of $\boldsymbol{\tau}$, belongs to $\mathbb{H}_h^{\boldsymbol{\sigma}}$. In this way, using again the first equation of the Galerkin scheme (2.16) and the compatibility condition (2.2) we deduce that $\mathcal{R}_1(c\,\mathbb{I})=0$, so that denoting

$$\widehat{\boldsymbol{\zeta}} := \boldsymbol{\zeta}-\boldsymbol{\Pi}_h^k(\boldsymbol{\zeta}) \quad \text{and} \quad \widehat{\boldsymbol{\xi}} := \boldsymbol{\xi}-\boldsymbol{\mathcal{I}}_h(\boldsymbol{\xi})\,,$$

it follows from (3.20) and (3.21), that

$$\mathcal{R}_1(\boldsymbol{\tau}) \,=\, \mathcal{R}_1(\boldsymbol{\tau}-\boldsymbol{\tau}_h) \,=\, \mathcal{R}_1(\widehat{\boldsymbol{\zeta}})+\mathcal{R}_1(\underline{\mathbf{curl}}(\widehat{\boldsymbol{\xi}}))\,, \tag{3.22}$$

where, according to the definition of $\mathcal{R}_1$ (cf. (3.16)), we find that

$$\mathcal{R}_1\big(\widehat{\boldsymbol{\zeta}}\big) \,=\, \Big\langle \widehat{\boldsymbol{\zeta}}\mathbf{n},\mathbf{u}_{\mathrm{D}}\Big\rangle_{\Gamma}-\int_\Omega \mathbf{u}_h\cdot\mathbf{div}(\widehat{\boldsymbol{\zeta}})-\frac{1}{\nu}\int_\Omega \big(\boldsymbol{\sigma}_h+(\mathbf{u}_h\otimes\mathbf{u}_h)\big)^{\mathrm{d}}:\widehat{\boldsymbol{\zeta}} \tag{3.23}$$

and

$$\mathcal{R}_1\big(\underline{\mathbf{curl}}(\widehat{\boldsymbol{\xi}})\big) \,=\, \Big\langle \underline{\mathbf{curl}}(\widehat{\boldsymbol{\xi}})\mathbf{n},\mathbf{u}_{\mathrm{D}}\Big\rangle_{\Gamma}-\frac{1}{\nu}\int_\Omega \big(\boldsymbol{\sigma}_h+(\mathbf{u}_h\otimes\mathbf{u}_h)\big)^{\mathrm{d}}:\underline{\mathbf{curl}}(\widehat{\boldsymbol{\xi}})\,. \tag{3.24}$$

The following lemma establishes the residual upper bound for $\|\mathcal{R}_1\|_{\mathbb{H}_0(\mathbf{div}_{4/3};\Omega)'}$.

Lemma 3.4 *Assume that $\mathbf{u}_{\mathrm{D}}\in\mathbf{H}^1(\Gamma)$. Then, there exists a positive constant C, independent of h, such that*

$$\|\mathcal{R}_1\|_{\mathbb{H}_0(\mathbf{div}_{4/3};\Omega)'} \,\leq\, C\left\{\left(\sum_{T\in\mathcal{T}_h}\Theta_{1,T}^4\right)^{1/4}+\left(\sum_{T\in\mathcal{T}_h}\Theta_{2,T}^2\right)^{1/2}\right\}, \tag{3.25}$$

where $\Theta_{1,T}$ and $\Theta_{2,T}$ are defined in (3.2) *and* (3.3)*, respectively.*

Proof. We proceed as in [8, Lemma 3.6] (see also [22, Lemma 3.7]). In fact, according to (3.22), we begin by estimating $\mathcal{R}_1(\widehat{\boldsymbol{\zeta}})$. Let us first observe that, for each $e\in\mathcal{E}_h$, the identity (A.6) and the fact

that $\mathbf{u}_h|_e \in \mathbf{P}_k(e)$, yield $\displaystyle\int_e \widehat{\boldsymbol{\zeta}}\mathbf{n}\cdot\mathbf{u}_h = 0$. Hence, locally integrating by parts the second term in (3.23), we readily obtain

$$\mathcal{R}_1(\widehat{\boldsymbol{\zeta}}) = \sum_{e\in\mathcal{E}_h(\Gamma)}\int_e (\mathbf{u}_{\mathrm{D}}-\mathbf{u}_h)\cdot\widehat{\boldsymbol{\zeta}}\mathbf{n} + \int_\Omega \left(\nabla\mathbf{u}_h - \frac{1}{\nu}\big(\boldsymbol{\sigma}_h + (\mathbf{u}_h\otimes\mathbf{u}_h)\big)^{\mathrm{d}}\right) : \widehat{\boldsymbol{\zeta}}\,.$$

Thus, applying the Hölder inequality along with the approximation properties of $\boldsymbol{\Pi}_h^k$ (cf. (A.10)–(A.11) in Lemma A.1) with $p = 4/3$ and $\ell = 0$, and the stability estimate (3.20), we find that

$$\begin{aligned}\big|\mathcal{R}_1(\widehat{\boldsymbol{\zeta}})\big| \;\leq\; \widehat{C}_1\left\{\sum_{T\in\mathcal{T}_h} h_T^4\left\|\nabla\mathbf{u}_h - \frac{1}{\nu}\big(\boldsymbol{\sigma}_h + (\mathbf{u}_h\otimes\mathbf{u}_h)\big)^{\mathrm{d}}\right\|^4_{0,4;T}\right.\\ \left. + \sum_{e\in\mathcal{E}_h(\Gamma)} h_e\,\|\mathbf{u}_{\mathrm{D}}-\mathbf{u}_h\|^4_{0,4;e}\right\}^{1/4}\|\boldsymbol{\tau}\|_{\mathbf{div}_{4/3};\Omega}\,.\end{aligned} \tag{3.26}$$

Next, we estimate $\mathcal{R}_1(\underline{\mathbf{curl}}(\widehat{\boldsymbol{\xi}}))$ (cf. (3.24)). In fact, regarding its first term, a suitable integration by parts formula on the boundary Γ, obtained from [24, Chapter I, eq. (2.17) and Theorem 2.11] (see also [17, Lemma 3.5, eq. (3.35) for 2D case]), yields

$$\Big\langle\underline{\mathbf{curl}}(\widehat{\boldsymbol{\xi}})\mathbf{n},\mathbf{u}_{\mathrm{D}}\Big\rangle_\Gamma \;=\; -\,\Big\langle\nabla\mathbf{u}_{\mathrm{D}}\times\mathbf{n},\widehat{\boldsymbol{\xi}}\Big\rangle_\Gamma \;=\; -\,\Big\langle\boldsymbol{\delta}_*\left(\nabla\mathbf{u}_{\mathrm{D}}\right),\widehat{\boldsymbol{\xi}}\Big\rangle_\Gamma\,. \tag{3.27}$$

In turn, locally integrating by parts the second term of $\mathcal{R}_1(\underline{\mathbf{curl}}(\widehat{\boldsymbol{\xi}}))$, we get

$$\begin{aligned}\frac{1}{\nu}\int_\Omega\big(\boldsymbol{\sigma}_h+(\mathbf{u}_h\otimes\mathbf{u}_h)\big)^{\mathrm{d}} : \underline{\mathbf{curl}}(\widehat{\boldsymbol{\xi}}) &= \sum_{T\in\mathcal{T}_h}\int_T \underline{\mathbf{curl}}\left(\frac{1}{\nu}\big(\boldsymbol{\sigma}_h+(\mathbf{u}_h\otimes\mathbf{u}_h)\big)^{\mathrm{d}}\right)\cdot\widehat{\boldsymbol{\xi}}\\ &- \sum_{e\in\mathcal{E}_h(\Omega)}\int_e\left[\left[\boldsymbol{\delta}_*\left(\frac{1}{\nu}\big(\boldsymbol{\sigma}_h+(\mathbf{u}_h\otimes\mathbf{u}_h)\big)^{\mathrm{d}}\right)\right]\right]\cdot\widehat{\boldsymbol{\xi}} - \sum_{e\in\mathcal{E}_h(\Gamma)}\int_e\boldsymbol{\delta}_*\left(\frac{1}{\nu}\big(\boldsymbol{\sigma}_h+(\mathbf{u}_h\otimes\mathbf{u}_h)\big)^{\mathrm{d}}\right)\cdot\widehat{\boldsymbol{\xi}}\,,\end{aligned}$$

which together with (3.27), the Cauchy–Schwarz inequality, the approximation properties of $\boldsymbol{\mathcal{I}}_h$ (cf. Lemma A.3), and again the stability estimate (3.20), implies

$$\begin{aligned}\big|\mathcal{R}_1(\underline{\mathbf{curl}}(\widehat{\boldsymbol{\xi}}))\big| \;\leq\; \widehat{C}_2\left\{\sum_{T\in\mathcal{T}_h} h_T^2\left\|\underline{\mathbf{curl}}\left(\frac{1}{\nu}\big(\boldsymbol{\sigma}_h+(\mathbf{u}_h\otimes\mathbf{u}_h)\big)^{\mathrm{d}}\right)\right\|^2_{0,T}\right.\\ + \sum_{e\in\mathcal{E}_h(\Omega)} h_e\left\|\left[\left[\boldsymbol{\delta}_*\left(\frac{1}{\nu}\big(\boldsymbol{\sigma}_h+(\mathbf{u}_h\otimes\mathbf{u}_h)\big)^{\mathrm{d}}\right)\right]\right]\right\|^2_{0,e}\\ \left. + \sum_{e\in\mathcal{E}_h(\Gamma)} h_e\left\|\boldsymbol{\delta}_*\left(\nabla\mathbf{u}_{\mathrm{D}}-\frac{1}{\nu}\big(\boldsymbol{\sigma}_h+(\mathbf{u}_h\otimes\mathbf{u}_h)\big)^{\mathrm{d}}\right)\right\|^2_{0,e}\right\}^{1/2}\|\boldsymbol{\tau}\|_{\mathbf{div}_{4/3};\Omega}\,.\end{aligned} \tag{3.28}$$

Finally, it is easy to see that (3.19), (3.22), (3.26), (3.28), and the definitions of the local estimators $\Theta_{1,T},\Theta_{2,T}$ (cf. (3.2), (3.3)) give (3.25), which ends the proof. □

We end this section by stressing that the reliability estimate (3.10) (cf. Theorem 3.1) follows by bounding the terms $\|\mathcal{R}_1\|_{\mathbb{H}_0(\mathbf{div}_{4/3};\Omega)'}$ and $\|\mathcal{R}_2\|_{\mathbf{L}^4(\Omega)'}$ in (3.18) by the corresponding upper bounds derived in Lemmas 3.3 and 3.4, and considering the definition of the global estimator Θ (cf. (3.1)).

3.2 Efficiency of the *a posteriori* error estimator

We now aim to establish the efficiency estimate of Θ (cf. (3.1)). For this purpose, we will make extensive use of the notations and results from Appendix B, and the original system of equations given by (2.5), which is recovered from the mixed continuous formulation (2.12) (cf. (2.7)) by choosing suitable test functions and integrating by parts backwardly the corresponding equations. The following theorem is the main result of this section.

Theorem 3.5 *Assume, for simplicity, that* $\mathbf{u}_{\mathrm{D}}$ *is piecewise polynomial. Then, there exists a positive constant* $C_{\mathtt{eff}}$*, independent of* h*, such that*

$$C_{\mathtt{eff}}\,\Theta \,+\, \mathtt{h.o.t.} \,\leq\, \|(\boldsymbol{\sigma},\mathbf{u})-(\boldsymbol{\sigma}_h,\mathbf{u}_h)\|_{\mathbf{X}}\,, \tag{3.29}$$

where `h.o.t.` *stands for one or several terms of higher order.*

Throughout this section we assume, without loss of generality, that $\mathbf{f}$ and $\mathbf{u}_{\mathrm{D}}$, are all piecewise polynomials. Otherwise, if $\mathbf{f}$ and $\mathbf{u}_{\mathrm{D}}$ are sufficiently smooth, one proceeds similarly to [11, Section 6.2], so that higher order terms given by the errors arising from suitable polynomial approximation of these functions appear in (3.29), which explains the eventual `h.o.t.` in this inequality.

We begin deriving the efficiency estimate (3.29) with the following result for the term defining $\Theta_{3,T}$ (cf. (3.4)).

Lemma 3.6 *There exists a positive constant* C_1*, independent of* h*, such that*

$$\begin{aligned}&\big\|\mathbf{f}+\mathbf{div}(\boldsymbol{\sigma}_h)-\mathtt{D}\,\mathbf{u}_h-\mathtt{F}\,|\mathbf{u}_h|^{\rho-2}\mathbf{u}_h\big\|^{4/3}_{0,4/3;T}\\ &\qquad\leq\, C_1\left\{\|\boldsymbol{\sigma}-\boldsymbol{\sigma}_h\|^{4/3}_{\mathbf{div}_{4/3};T}+\|\mathbf{u}-\mathbf{u}_h\|^{4/3}_{0,4;T}+\big\||\mathbf{u}|^{\rho-2}\mathbf{u}-|\mathbf{u}_h|^{\rho-2}\mathbf{u}_h\big\|^{4/3}_{0,4/3;T}\right\}\quad\forall\, T\in\mathcal{T}_h\,.\end{aligned}$$

Proof. It suffices to recall that $\mathtt{D}\,\mathbf{u}+\mathtt{F}\,|\mathbf{u}|^{\rho-2}\mathbf{u}-\mathbf{div}(\boldsymbol{\sigma})=\mathbf{f}$ in Ω (cf. (2.5)) and apply triangle inequality. We omit further details. □

Now we proceed by deriving the estimates for the terms defining $\Theta_{1,T}$ (cf. (3.2)).

Lemma 3.7 *There exists a positive constant* C_2*, independent of* h*, such that*

$$\begin{aligned}&h_T^4\,\left\|\nabla\mathbf{u}_h-\frac{1}{\nu}\big(\boldsymbol{\sigma}_h+(\mathbf{u}_h\otimes\mathbf{u}_h)\big)^{\mathrm{d}}\right\|^4_{0,4;T}\\ &\qquad\leq\, C_2\left\{h_T^2\,\|\boldsymbol{\sigma}-\boldsymbol{\sigma}_h\|^4_{0,T}+\|\mathbf{u}-\mathbf{u}_h\|^4_{0,4;T}+h_T^2\,\|\mathbf{u}\otimes\mathbf{u}-\mathbf{u}_h\otimes\mathbf{u}_h\|^4_{0,T}\right\}\quad\forall\, T\in\mathcal{T}_h\,.\end{aligned}\tag{3.30}$$

Proof. We proceed as in the proof of [9, Lemma 5.15]. In fact, given $T\in\mathcal{T}_h$, we begin by applying the tensor version of the left-hand side inequality of (B.2) (cf. Lemma B.1), with $p=4$ and $q=4/3$, to the local polinomial $\boldsymbol{\chi}_T:=\nabla\mathbf{u}_h-\frac{1}{\nu}\big(\boldsymbol{\sigma}_h+(\mathbf{u}_h\otimes\mathbf{u}_h)\big)^{\mathrm{d}}\in\mathbb{P}_k(T)$, which gives

$$c_1\,\|\boldsymbol{\chi}_T\|_{0,4;T}\,\leq\,\sup_{\mathbf{0}\neq\boldsymbol{\tau}\in\mathbb{P}_k(T)}\frac{\displaystyle\int_T\boldsymbol{\chi}_T:(\psi_T\boldsymbol{\tau})}{\|\boldsymbol{\tau}\|_{0,4/3;T}}\,.\tag{3.31}$$

Then, using the identity $\nabla\mathbf{u} = \dfrac{1}{\nu}\,(\boldsymbol{\sigma} + (\mathbf{u}\otimes\mathbf{u}))^{\mathrm{d}}$ in Ω (cf.(2.5)), and integrating by parts along with (B.1), we find that

$$\begin{aligned}\int_T \boldsymbol{\chi}_T : (\psi_T\boldsymbol{\tau}) \;&=\; \int_T \Big\{\nabla(\mathbf{u}_h - \mathbf{u}) + \frac{1}{\nu}\big((\boldsymbol{\sigma}-\boldsymbol{\sigma}_h) + (\mathbf{u}\otimes\mathbf{u} - \mathbf{u}_h\otimes\mathbf{u}_h)\big)^{\mathrm{d}}\Big\} : \psi_T\boldsymbol{\tau} \\ &=\; \int_T (\mathbf{u}-\mathbf{u}_h)\cdot\mathbf{div}(\psi_T\boldsymbol{\tau}) + \int_T \frac{1}{\nu}\big((\boldsymbol{\sigma}-\boldsymbol{\sigma}_h) + (\mathbf{u}\otimes\mathbf{u} - \mathbf{u}_h\otimes\mathbf{u}_h)\big)^{\mathrm{d}} : \psi_T\boldsymbol{\tau}\,,\end{aligned}$$

from which, employing the Hölder and Cauchy-Schwarz inequalities, noting that

$$\|\mathbf{div}(\psi_T\boldsymbol{\tau})\|_{0,4/3;T} \;\leq\; \|\nabla(\psi_T\boldsymbol{\tau})\|_{0,4/3;T}$$

and then applying the right-hand side inequality of (B.3), along with the fact that $0 \leq \psi_T \leq 1$, we obtain

$$\begin{aligned}\int_T \boldsymbol{\chi}_T : (\psi_T\boldsymbol{\tau}) \;&\leq\; c_3\, h_T^{-1}\,\|\mathbf{u}-\mathbf{u}_h\|_{0,4;T}\|\boldsymbol{\tau}\|_{0,4/3;T} \\ &\quad + \frac{1}{\nu}\Big(\|\boldsymbol{\sigma}-\boldsymbol{\sigma}_h\|_{0,T} + \|\mathbf{u}\otimes\mathbf{u} - \mathbf{u}_h\otimes\mathbf{u}_h\|_{0,T}\Big)\|\boldsymbol{\tau}\|_{0,T}\,.\end{aligned} \tag{3.32}$$

In turn, according to the local inverse inequality (B.4) (cf. Lemma B.2) with $d=2$, $\ell = m = 0$, $r = 2$, and $s = 4/3$, there holds

$$\|\boldsymbol{\tau}\|_{0,T} \;\leq\; c\, h_T^{-1/2}\,\|\boldsymbol{\tau}\|_{0,4/3;T}\,,$$

and thus (3.32) becomes

$$\int_T \boldsymbol{\chi}_T : (\psi_T\boldsymbol{\tau}) \;\leq\; C\,\Big\{h_T^{-1}\,\|\mathbf{u}-\mathbf{u}_h\|_{0,4;T} + h^{-1/2}\Big(\|\boldsymbol{\sigma}-\boldsymbol{\sigma}_h\|_{0,T} + \|\mathbf{u}\otimes\mathbf{u} - \mathbf{u}_h\otimes\mathbf{u}_h\|_{0,T}\Big)\Big\}\,\|\boldsymbol{\tau}\|_{0,4/3;T}\,,$$

which replaced back into (3.31), and multiplying the resulting inequality by h_T, we get

$$\begin{aligned}&h_T\,\Big\|\nabla\mathbf{u}_h - \frac{1}{\nu}\big(\boldsymbol{\sigma}_h + (\mathbf{u}_h\otimes\mathbf{u}_h)\big)^{\mathrm{d}}\Big\|_{0,4;T} \\ &\quad\leq\; C\Big\{\|\mathbf{u}-\mathbf{u}_h\|_{0,4;T} + h_T^{1/2}\,\|\boldsymbol{\sigma}-\boldsymbol{\sigma}_h\|_{0,T} + h_T^{1/2}\,\|\mathbf{u}\otimes\mathbf{u} - \mathbf{u}_h\otimes\mathbf{u}_h\|_{0,T}\Big\}\,,\end{aligned}$$

so that taking the foregoing inequality to the power 4 the required bound is obtained. □

The remaining local efficiency estimate for $\Theta_{1,T}$ (cf. (3.2)) is established as follows.

Lemma 3.8 *Assume that $\mathbf{u}_{\mathrm{D}}$ is piecewise polynomial. Then, there exists a positive constant $C_3 > 0$, independent of h, such that*

$$h_e\,\|\mathbf{u}_{\mathrm{D}} - \mathbf{u}_h\|^4_{0,4;e} \;\leq\; C_3\,\Big\{h_{T_e}^2\,\|\boldsymbol{\sigma}-\boldsymbol{\sigma}_h\|^4_{0,T_e} + \|\mathbf{u}-\mathbf{u}_h\|^4_{0,4;T_e} + h_{T_e}^2\,\|\mathbf{u}\otimes\mathbf{u} - \mathbf{u}_h\otimes\mathbf{u}_h\|^4_{0,T_e}\Big\}\,,$$

for all $e \in \mathcal{E}_h(\Gamma)$, and where T_e is the triangle/tetrahedron of $\mathcal{T}_h$ having e as an edge/face.

Proof. It follows from a slight adaptation of [22, Lemma 3.16], we include the proof for the sake of completeness. In fact, given $e \in \mathcal{E}_h(\Gamma)$, we first observe that the local inverse inequality (B.4) with $d = 1, \ell = m = 0, r = 4$, and $s = 2$, and the fact that $\mathbf{u} = \mathbf{u}_{\mathrm{D}}$ on Γ, yields $\|\mathbf{u}_{\mathrm{D}} - \mathbf{u}_h\|_{0,4;e} \leq c\, h_e^{-1/4}\,\|\mathbf{u}-\mathbf{u}_h\|_{0,e}$. Hence, taking the above to the power 4, applying the vector version of the discrete

trace inequality (B.5) (cf. Lemma B.3) with $p = 2$, recalling that $\frac{1}{\nu}\big(\boldsymbol{\sigma} + (\mathbf{u}\otimes\mathbf{u})\big)^{\mathrm{d}} = \nabla\mathbf{u}$ in Ω, employing the triangle inequality and some algebraic computations, we find that

$$
\begin{aligned}
h_e\,\|\mathbf{u}_{\mathrm{D}} - \mathbf{u}_h\|^4_{0,4;e} \,\leq\, C\,\left\{ h_{T_e}^{-1}\,\|\mathbf{u}-\mathbf{u}_h\|^2_{0,T_e} + h_{T_e}\,\left\|\frac{1}{\nu}\big(\boldsymbol{\sigma}+(\mathbf{u}\otimes\mathbf{u})\big)^{\mathrm{d}} - \nabla\mathbf{u}_h\right\|^2_{0,T_e}\right\}^2 \\
\leq\, C\,\left\{ h_{T_e}^{-2}\,\|\mathbf{u}-\mathbf{u}_h\|^4_{0,T_e} + h_{T_e}^2\,\|\boldsymbol{\sigma}-\boldsymbol{\sigma}_h\|^4_{0,T_e}\right. \qquad (3.33)\\
\left. + h_{T_e}^2\,\|\mathbf{u}\otimes\mathbf{u}-\mathbf{u}_h\otimes\mathbf{u}_h\|^4_{0,T_e} + h_{T_e}^2\,\left\|\nabla\mathbf{u}_h - \frac{1}{\nu}\big(\boldsymbol{\sigma}+(\mathbf{u}\otimes\mathbf{u})\big)^{\mathrm{d}}\right\|^4_{0,T_e}\right\}.
\end{aligned}
$$

Next, and owing to Cauchy–Schwarz's inequality and the fact that $|T_e| \cong h_{T_e}^d$, with $d \in \{2,3\}$, we have that

$$
\|\mathbf{w}\|^4_{0,T_e} \,\leq\, |T_e|\,\|\mathbf{w}\|^4_{0,4;T_e} \,\leq\, c\,h_{T_e}^d\,\|\mathbf{w}\|^4_{0,4;T_e} \,\leq\, c\,h_{T_e}^2\,\|\mathbf{w}\|^4_{0,4;T_e} \quad \forall\,\mathbf{w}\in\mathbf{L}^4(T_e)
$$

and it follows from (3.33) that

$$
\begin{aligned}
h_e\,\|\mathbf{u}_{\mathrm{D}} - \mathbf{u}_h\|^4_{0,4;e} \,\leq\, C\,\left\{ \|\mathbf{u}-\mathbf{u}_h\|^4_{0,4;T_e} + h_{T_e}^2\,\|\boldsymbol{\sigma}-\boldsymbol{\sigma}_h\|^4_{0,T_e}\right. \\
\left. + h_{T_e}^2\,\|\mathbf{u}\otimes\mathbf{u}-\mathbf{u}_h\otimes\mathbf{u}_h\|^4_{0,T_e} + h_{T_e}^4\,\left\|\nabla\mathbf{u}_h - \frac{1}{\nu}\big(\boldsymbol{\sigma}+(\mathbf{u}\otimes\mathbf{u})\big)^{\mathrm{d}}\right\|^4_{0,4;T_e}\right\}.
\end{aligned}
$$

Finally, as a consequence of (3.30) (cf. Lemma 3.7) we can bound the last term in the foregoing inequality, and this step concludes the proof. □

The corresponding bounds for the terms defining $\Theta_{2,T}$ (cf. (3.3)) are stated in the following lemma.

Lemma 3.9 *There exist $C_4 > 0$ and $C_5 > 0$, independent of h, such that*

$$
h_T^2\,\left\|\underline{\mathbf{curl}}\left(\frac{1}{\nu}\big(\boldsymbol{\sigma}_h + (\mathbf{u}_h\otimes\mathbf{u}_h)\big)^{\mathrm{d}}\right)\right\|^2_{0,T} \,\leq\, C_4\left\{\|\boldsymbol{\sigma}-\boldsymbol{\sigma}_h\|^2_{0,T} + \|\mathbf{u}\otimes\mathbf{u}-\mathbf{u}_h\otimes\mathbf{u}_h\|^2_{0,T}\right\} \qquad (3.34)
$$

for all $T \in \mathcal{T}_h$ and

$$
h_e\,\left\|\left[\left[\boldsymbol{\delta}_*\left(\frac{1}{\nu}\big(\boldsymbol{\sigma}_h + (\mathbf{u}_h\otimes\mathbf{u}_h)\big)^{\mathrm{d}}\right)\right]\right]\right\|^2_{0,e} \,\leq\, C_5\left\{\|\boldsymbol{\sigma}-\boldsymbol{\sigma}_h\|^2_{0,\omega_e} + \|\mathbf{u}\otimes\mathbf{u}-\mathbf{u}_h\otimes\mathbf{u}_h\|^2_{0,\omega_e}\right\} \qquad (3.35)
$$

for all $e \in \mathcal{E}_h(\Omega)$, where ω_e denotes the union of the two elements of $\mathcal{T}_h$ sharing the edge/face e. Additionally, if $\mathbf{u}_{\mathrm{D}}$ is piecewise polynomial, there exists $C_6 > 0$, independent of h, such that

$$
h_e\,\left\|\boldsymbol{\delta}_*\left(\nabla\mathbf{u}_{\mathrm{D}} - \frac{1}{\nu}\big(\boldsymbol{\sigma}_h + (\mathbf{u}_h\otimes\mathbf{u}_h)\big)^{\mathrm{d}}\right)\right\|^2_{0,e} \,\leq\, C_6\left\{\|\boldsymbol{\sigma}-\boldsymbol{\sigma}_h\|^2_{0,T_e} + \|\mathbf{u}\otimes\mathbf{u}-\mathbf{u}_h\otimes\mathbf{u}_h\|^2_{0,T_e}\right\} \qquad (3.36)
$$

for all $e \in \mathcal{E}_h(\Gamma)$, where T_e is the element to which the boundary edge/face e belongs.

Proof. First, noting that $\underline{\mathbf{curl}}\left(\frac{1}{\nu}\big(\boldsymbol{\sigma} + (\mathbf{u}\otimes\mathbf{u})\big)^{\mathrm{d}}\right) = \underline{\mathbf{curl}}\,(\nabla\mathbf{u}) = \mathbf{0}$ in Ω, we find that (3.34)–(3.35) follows from a slight adaptation of [23, Lemma 4.11], whereas for the proof of (3.36) we refer the reader to [23, Lemma 4.15]. □

In order to complete the global efficiency given by (3.29) (cf. Theorem 3.5), we now need to estimate the terms $\big\||\mathbf{u}|^{\rho-2}\mathbf{u}-|\mathbf{u}_h|^{\rho-2}\mathbf{u}_h\big\|^{4/3}_{0,4/3;T}$ and $\|\mathbf{u}\otimes\mathbf{u}-\mathbf{u}_h\otimes\mathbf{u}_h\|^{j}_{0,T}$, with $j\in\{2,4\}$, appearing in the upper bounds provided by Lemmas 3.6 and 3.7–3.9, respectively. To this end, we first make use of (3.7) with $m=\rho$, the Hölder inequality with $p=3/2$ and $q=3$ satisfying $1/p+1/q=1$, and simple algebraic manipulations, to obtain

$$\big\||\mathbf{u}|^{\rho-2}\mathbf{u}-|\mathbf{u}_h|^{\rho-2}\mathbf{u}_h\big\|^{4/3}_{0,4/3;T}\,\leq\,\widehat{c}_\rho\,\Big(\|\mathbf{u}\|^{4(\rho-2)/3}_{0,2(\rho-2);T}+\|\mathbf{u}_h\|^{4(\rho-2)/3}_{0,2(\rho-2);T}\Big)\|\mathbf{u}-\mathbf{u}_h\|^{4/3}_{0,4;T}\,,$$

with $\widehat{c}_\rho$ depending on ρ. Then, applying Hölder inequality and some algebraic computations, we find that

$$\begin{aligned}
&\sum_{T\in\mathcal{T}_h}\big\||\mathbf{u}|^{\rho-2}\mathbf{u}-|\mathbf{u}_h|^{\rho-2}\mathbf{u}_h\big\|^{4/3}_{0,4/3;T}\\
&\quad\leq\,\widehat{c}_\rho\,\left\{\sum_{T\in\mathcal{T}_h}\Big(\|\mathbf{u}\|^{4(\rho-2)/3}_{0,2(\rho-2);T}+\|\mathbf{u}_h\|^{4(\rho-2)/3}_{0,2(\rho-2);T}\Big)^{3/2}\right\}^{2/3}\,\left\{\sum_{T\in\mathcal{T}_h}\|\mathbf{u}-\mathbf{u}_h\|^4_{0,4;T}\right\}^{1/3}\\
&\quad\leq\,\sqrt[3]{2}\,\widehat{c}_\rho\,\Big(\|\mathbf{u}\|^{4(\rho-2)/3}_{0,2(\rho-2);\Omega}+\|\mathbf{u}_h\|^{4(\rho-2)/3}_{0,2(\rho-2);\Omega}\Big)\|\mathbf{u}-\mathbf{u}_h\|^{4/3}_{0,4;\Omega}\,.
\end{aligned}\tag{3.37}$$

In this way, using the Sobolev embedding of $\mathbf{L}^4(\Omega)$ into $\mathbf{L}^{2(\rho-2)}(\Omega)$, with $2(\rho-2)\in[2,4]$, and the fact that $\mathbf{u}\in\mathbf{W}_r$ and $\mathbf{u}_h\in\mathbf{W}_{\widetilde{r}}$, we deduce from (3.37) that there exists a constant $C>0$, depending only on $r,\widetilde{r}$ and other constants, and hence independent of h, such that

$$\sum_{T\in\mathcal{T}_h}\big\||\mathbf{u}|^{\rho-2}\mathbf{u}-|\mathbf{u}_h|^{\rho-2}\mathbf{u}_h\big\|^{4/3}_{0,4/3;T}\,\leq\,C\,\|\mathbf{u}-\mathbf{u}_h\|^{4/3}_{0,4;\Omega}\,.\tag{3.38}$$

Similarly, adding and subtracting $\mathbf{u}\otimes\mathbf{u}_h$ (it also works with $\mathbf{u}_h\otimes\mathbf{u}$), and applying Cauch–Schwarz's inequality, we deduce that

$$\|\mathbf{u}\otimes\mathbf{u}-\mathbf{u}_h\otimes\mathbf{u}_h\|_{0,T}\,\leq\,\big(\|\mathbf{u}\|_{0,4;T}+\|\mathbf{u}_h\|_{0,4;T}\big)\|\mathbf{u}-\mathbf{u}_h\|_{0,4;T}\,,$$

so that proceeding analogously to (3.37) and using again the fact that $\mathbf{u}\in\mathbf{W}_r$ and $\mathbf{u}_h\in\mathbf{W}_{\widetilde{r}}$, we are able to show that there exists a positive constant $\widetilde{C}$, independent of h, such that

$$\sum_{T\in\mathcal{T}_h}\|\mathbf{u}\otimes\mathbf{u}-\mathbf{u}_h\otimes\mathbf{u}_h\|^4_{0,T}\,\leq\,\widetilde{C}\,\|\mathbf{u}-\mathbf{u}_h\|^4_{0,4;\Omega}\,.\tag{3.39}$$

The case of (3.39) with exponent $j=2$ is analogous. Consequently, it is not difficult to see that (3.29) follows from the definition of Θ (cf. (3.1)–(3.4)), Lemmas 3.6, 3.7, 3.8, and 3.9, and the estimates (3.38) and (3.39).

4 Numerical results

This section serves to illustrate the performance and accuracy of the mixed finite element scheme (2.16) (cf. (2.17)) along with the reliability and efficiency properties of the *a posteriori* error estimator Θ (cf. (3.1)) derived in Section 3. In what follows, we refer to the corresponding sets of finite element subspaces generated by $k=0$ and $k=1$, as simply $\mathbb{RT}_0-\mathbf{P}_0$ and $\mathbb{RT}_1-\mathbf{P}_1$, respectively. The implementation is based on a `FreeFem++` code [26]. Regarding the implementation of the Newton iterative method associated to (2.16) (see [7, eq. (6.1) in Section 6] for details), the iterations are

terminated once the relative error of the entire coefficient vectors between two consecutive iterates, say $\mathbf{coeff}^m$ and $\mathbf{coeff}^{m+1}$, is sufficiently small, i.e.,

$$\frac{\|\mathbf{coeff}^{m+1} - \mathbf{coeff}^m\|_{\mathtt{DoF}}}{\|\mathbf{coeff}^{m+1}\|_{\mathtt{DoF}}} \leq \mathsf{tol},$$

where $\|\cdot\|_{\mathtt{DoF}}$ stands for the usual Euclidean norm in $\mathrm{R}^{\mathtt{DoF}}$, with $\mathtt{DoF}$ denoting the total number of degrees of freedom defining the finite element subspaces $\mathbb{H}_h^{\boldsymbol{\sigma}}$ and $\mathbf{H}_h^{\mathbf{u}}$ stated in Section 2.3, and tol is a fixed tolerance chosen as tol=1E-06.

The global error and the effectivity index associated to the global estimator Θ (cf. (3.1)) are denoted, respectively, by

$$\mathsf{e}(\boldsymbol{\sigma}, \mathbf{u}) := \mathsf{e}(\boldsymbol{\sigma}) + \mathsf{e}(\mathbf{u}) \quad \text{and} \quad \mathtt{eff}(\Theta) := \frac{\mathsf{e}(\boldsymbol{\sigma}, \mathbf{u})}{\Theta},$$

where

$$\mathsf{e}(\boldsymbol{\sigma}) := \|\boldsymbol{\sigma} - \boldsymbol{\sigma}_h\|_{\mathbf{div}_{4/3};\Omega} \quad \text{and} \quad \mathsf{e}(\mathbf{u}) := \|\mathbf{u} - \mathbf{u}_h\|_{0,4;\Omega}.$$

We emphasize that other variables of physical interest such as the pressure, velocity gradient, vorticity and shear stress tensor can be computed using the postprocessing formulae detailed in [7, Section 5]. However, for the sake of simplicity, we only present some plots in Examples 2–4 for the pressure and velocity gradient (cf. (2.4) and [7, eq. (5.8)]), using the formulae

$$p_h := -\frac{1}{d}\,\mathrm{tr}(\boldsymbol{\sigma}_h + \mathbf{u}_h \otimes \mathbf{u}_h) + \frac{1}{d\,|\Omega|}\int_\Omega \mathrm{tr}(\mathbf{u}_h \otimes \mathbf{u}_h) \quad \text{and} \quad \mathbf{G}_h := \frac{1}{\nu}\left(\boldsymbol{\sigma}_h^{\mathrm{d}} + (\mathbf{u}_h \otimes \mathbf{u}_h)^{\mathrm{d}}\right).$$

Moreover, using the fact that $\mathtt{DoF}^{-1/d} \cong h$, the respective experimental rates of convergence are computed as

$$\mathsf{r}(\diamond) := -d\,\frac{\log(\mathsf{e}(\diamond)/\mathsf{e}'(\diamond))}{\log(\mathtt{DoF}/\mathtt{DoF}')} \quad \text{for each } \diamond \in \left\{\boldsymbol{\sigma}, \mathbf{u}, (\boldsymbol{\sigma}, \mathbf{u})\right\},$$

where $\mathtt{DoF}$ and $\mathtt{DoF}'$ denote the total degrees of freedom associated to two consecutive triangulations with errors e and e', respectively.

The examples to be considered in this section are described next. In all of them, for sake of simplicity, we take $\nu = 1$. In turn, in the first three examples we consider the parameters $\mathtt{F} = 10$ and $\mathtt{D} = 1$. In addition, the null mean value of $\mathrm{tr}(\boldsymbol{\sigma}_h)$ over Ω is fixed via a real Lagrange multiplier strategy.

Example 1 is used to corroborate the reliability and efficiency of the *a posteriori* error estimator Θ, whereas Examples 2, 3 and 4 are utilized to illustrate the behavior of the associated adaptive algorithm in 2D and 3D domains with and without manufactured solution, respectively, which applies the following procedure from [30]:

(1) Start with a coarse mesh $\mathcal{T}_h$.

(2) Solve the Newton iterative method associated to (2.16) for the current mesh $\mathcal{T}_h$.

(3) Compute the local indicator Θ_T for each $T \in \mathcal{T}_h$, where

$$\Theta_T := \Theta_{1,T} + \Theta_{2,T} + \Theta_{3,T}, \quad \text{(cf. (3.2), (3.3), (3.4))}$$

(4) Check the stopping criterion and decide whether to finish or go to next step.

$\mathbb{RT}_0 - \mathbf{P}_0$ scheme with quasi-uniform refinement										
DoF	h	it	$\mathsf{e}(\boldsymbol{\sigma})$	$\mathsf{r}(\boldsymbol{\sigma})$	$\mathsf{e}(\mathbf{u})$	$\mathsf{r}(\mathbf{u})$	$\mathsf{e}(\boldsymbol{\sigma},\mathbf{u})$	$\mathsf{r}(\boldsymbol{\sigma},\mathbf{u})$	Θ	$\mathtt{eff}(\Theta)$
196	0.373	4	4.43E-00	–	2.49E-01	–	4.68E-00	–	9.34E-00	0.501
792	0.196	4	1.94E-00	1.179	1.09E-01	1.185	2.05E-00	1.179	4.34E-00	0.473
3084	0.098	4	9.72E-01	1.020	5.45E-02	1.017	1.03E-00	1.020	2.22E-00	0.463
12208	0.048	4	4.74E-01	1.042	2.63E-02	1.059	5.01E-01	1.043	1.11E-00	0.452
48626	0.028	4	2.40E-01	0.989	1.34E-02	0.978	2.53E-01	0.988	5.55E-01	0.455
196242	0.014	4	1.19E-01	1.008	6.63E-03	1.007	1.25E-01	1.008	2.76E-01	0.454

$\mathbb{RT}_1 - \mathbf{P}_1$ scheme with quasi-uniform refinement										
DoF	h	it	$\mathsf{e}(\boldsymbol{\sigma})$	$\mathsf{r}(\boldsymbol{\sigma})$	$\mathsf{e}(\mathbf{u})$	$\mathsf{r}(\mathbf{u})$	$\mathsf{e}(\boldsymbol{\sigma},\mathbf{u})$	$\mathsf{r}(\boldsymbol{\sigma},\mathbf{u})$	Θ	$\mathtt{eff}(\Theta)$
608	0.373	4	5.31E-01	–	2.66E-02	–	5.57E-01	–	1.73E-00	0.323
2496	0.196	4	1.23E-01	2.073	6.68E-03	1.959	1.29E-01	2.068	3.88E-01	0.334
9792	0.098	4	3.12E-02	2.003	1.67E-03	2.026	3.29E-02	2.004	9.84E-02	0.334
38912	0.048	4	7.90E-03	1.993	4.32E-04	1.962	8.33E-03	1.991	2.44E-02	0.342
155296	0.028	4	1.99E-03	1.995	1.08E-04	1.999	2.09E-03	1.995	6.19E-03	0.338
627360	0.014	4	4.83E-04	2.025	2.63E-05	2.027	5.10E-04	2.025	1.51E-03	0.337

Table 4.1: [Example 1] Number of degrees of freedom, meshsizes, Newton iteration count, errors, rates of convergence, global estimator, and effectivity index for the $\mathbb{RT}_k - \mathbf{P}_k$ mixed approximations, with $k \in \{0,1\}$, for the convective Brinkman–Forchheimer model with $\rho = 3$.

(5) Use the automatic meshing algorithm adaptmesh from [27, Section 9.1.9] to refine each $T' \in \mathcal{T}_h$ satisfying:

$$\Theta_{T'} \geq C_{\mathsf{adm}} \frac{1}{\#T} \sum_{T \in \mathcal{T}_h} \Theta_T, \quad \text{for some } C_{\mathsf{adm}} \in (0,1), \tag{4.1}$$

where $\#T$ denotes the number of triangles of the mesh $\mathcal{T}_h$.

(6) Define resulting mesh as current mesh $\mathcal{T}_h$, and go to step (2).

In particular, in Examples 2 and 4 below we take $C_{\mathsf{adm}} = 0.8$ (cf. (4.1)), whereas for Example 3 we choose $C_{\mathsf{adm}} = 0.85$.

Example 1: Accuracy assessment with a smooth solution in a square domain.

In the first example, we concentrate on the accuracy of the mixed method (2.16). The domain is the square $\Omega := (0,1)^2$. We choose the inertial power $\rho = 3$, and adjust the data $\mathbf{f}$ and $\mathbf{u}_{\mathrm{D}}$ such that a manufactured solution of (2.5) is given by the smooth functions

$$\mathbf{u}(\mathbf{x}) := \begin{pmatrix} \sin(\pi\, x_1)\cos(\pi\, x_2) \\ -\cos(\pi\, x_1)\sin(\pi\, x_2) \end{pmatrix} \quad \text{and} \quad p(\mathbf{x}) := \cos(\pi\, x_1)\sin\left(\frac{\pi}{2}\, x_2\right).$$

The errors and associated rates of convergence are reported in Table 4.1, which are in accordance with the theoretical bounds established in [7, Theorem 4]. In addition, we also compute the global *a posteriori* error indicator Θ (cf. (3.1)), and measure its reliability and efficiency with the effectivity index. Notice that the estimator remain always bounded.

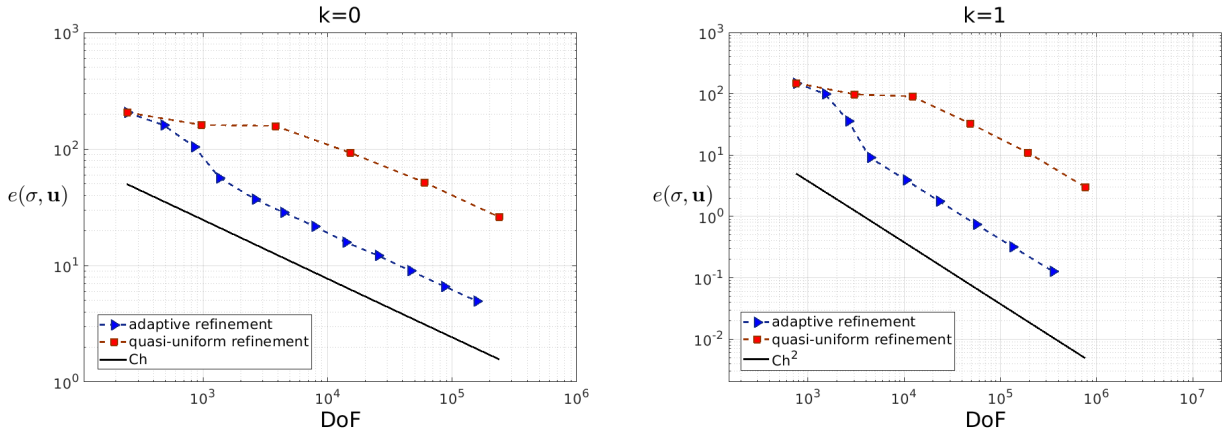

Figure 4.1: [Example 2] Log-log plot of $\mathtt{e}(\boldsymbol{\sigma}, \mathbf{u})$ vs. DoF for quasi-uniform/adaptive refinements for $k = 0$ and $k = 1$ (left and right plots, respectively).

Example 2: Adaptivity in a 2D four-to-one contraction domain.

The second example is aimed at testing the features of adaptive mesh refinement after the *a posteriori* error estimator Θ (cf. (3.1)). We consider a 2D four-to-one contraction domain $\Omega := (0, 2) \times (0, 1) \setminus (1, 2) \times (0.25, 1)$ and parameter $\rho = 3.5$. The data $\mathbf{f}$ and $\mathbf{u}_{\mathrm{D}}$ are chosen so that the exact solution is given by

$$\mathbf{u}(\mathbf{x}) := \begin{pmatrix} -\cos(\pi x_1)\sin(\pi x_2) \\ \sin(\pi x_1)\cos(\pi x_2) \end{pmatrix} \quad \text{and} \quad p(\mathbf{x}) := \frac{10\,(x_2 - 0.25)}{(x_1 - 1.02)^2 + (x_2 - 0.27)^2} - p_0\,,$$

where $p_0 \in \mathrm{R}$ is a constant chosen in such a way $\int_\Omega p = 0$. Notice that the pressure exhibit high gradients near the vertex $(1, 0.25)$.

Tables 4.2 and 4.3 along with Figure 4.1, summarizes the convergence history of the method applied to a sequence of quasi-uniformly and adaptively refined triangulation of the domain. Suboptimal rates are observed in the first case, whereas adaptive refinement according to the *a posteriori* error indicator Θ yields optimal convergence and stable effectivity indexes. Notice how the adaptive algorithms improves the efficiency of the method by delivering quality solutions at a lower computational cost, to the point that it is possible to get a better one (in terms of $\mathtt{e}(\boldsymbol{\sigma}, \mathbf{u})$) with approximately only the 3% of the degrees of freedom of the last quasi-uniform mesh for the mixed scheme in both cases $k = 0$ and $k = 1$. Furthermore, the initial mesh and approximate solutions built using the adaptive $\mathbb{RT}_1 - \mathbf{P}_1$ scheme (via Θ) with $351,102$ degrees of freedom and $21,879$ triangles, are shown in Figure 4.2. We observe there that the pressure exhibits high gradients in the contraction region. In turn, examples of some adapted meshes for $k = 0$ and $k = 1$ are collected in Figure 4.3. We notice a clear clustering of elements near the corner region of the contraction of the 2D four-to-one domain as we expected.

Example 3: Adaptivity in a 3D L-shape domain.

Here, we replicate the Example 2 in a three-dimensional setting but now considering the 3D L-shape domain $\Omega := (-0.5, 0.5) \times (0, 0.5) \times (-0.5, 0.5) \setminus (0, 0.5)^3$, the parameter $\rho = 4$, and the manufactured

$\mathbb{RT}_0 - \mathbf{P}_0$ scheme with quasi-uniform refinement										
DoF	h	it	$\mathsf{e}(\boldsymbol{\sigma})$	$\mathsf{r}(\boldsymbol{\sigma})$	$\mathsf{e}(\mathbf{u})$	$\mathsf{r}(\mathbf{u})$	$\mathsf{e}(\boldsymbol{\sigma},\mathbf{u})$	$\mathsf{r}(\boldsymbol{\sigma},\mathbf{u})$	Θ	$\mathtt{eff}(\Theta)$
244	0.373	5	2.05E+02	–	1.03E-00	–	2.06E+02	–	2.33E+02	0.882
968	0.206	4	1.60E+02	0.356	5.37E-01	0.938	1.61E+02	0.359	1.79E+02	0.897
3816	0.103	4	1.57E+02	0.030	4.34E-01	0.310	1.57E+02	0.030	1.71E+02	0.920
15062	0.049	4	9.28E+01	0.766	1.42E-01	1.633	9.30E+01	0.767	1.03E+02	0.899
59734	0.026	4	5.17E+01	0.850	5.20E-02	1.455	5.17E+01	0.851	5.87E+01	0.882
238498	0.013	4	2.60E+01	0.991	1.46E-02	1.838	2.60E+01	0.992	3.00E+01	0.869

$\mathbb{RT}_0 - \mathbf{P}_0$ scheme with adaptive refinement via Θ									
DoF	it	$\mathsf{e}(\boldsymbol{\sigma})$	$\mathsf{r}(\boldsymbol{\sigma})$	$\mathsf{e}(\mathbf{u})$	$\mathsf{r}(\mathbf{u})$	$\mathsf{e}(\boldsymbol{\sigma},\mathbf{u})$	$\mathsf{r}(\boldsymbol{\sigma},\mathbf{u})$	Θ	$\mathtt{eff}(\Theta)$
244	5	2.05E+02	–	1.03E-00	–	2.06E+02	–	2.33E+02	0.882
480	4	1.60E+02	0.732	4.70E-01	2.306	1.60E+02	0.738	1.74E+02	0.920
848	4	1.05E+02	1.489	2.26E-01	2.572	1.05E+02	1.492	1.17E+02	0.894
1350	4	5.64E+01	2.657	2.07E-01	0.373	5.66E+01	2.651	6.63E+01	0.855
2592	4	3.70E+01	1.290	1.43E-01	1.144	3.72E+01	1.290	4.43E+01	0.840
4386	4	2.85E+01	0.998	1.13E-01	0.880	2.86E+01	0.997	3.42E+01	0.837
7784	4	2.18E+01	0.942	7.95E-02	1.233	2.18E+01	0.943	2.61E+01	0.838
13816	4	1.59E+01	1.095	5.88E-02	1.053	1.59E+01	1.095	1.92E+01	0.830
25198	4	1.21E+01	0.895	4.21E-02	1.109	1.22E+01	0.895	1.46E+01	0.835
45852	4	8.98E-00	1.008	2.91E-02	1.238	9.01E-00	1.009	1.08E+01	0.834
85656	4	6.63E-00	0.970	2.08E-02	1.079	6.65E-00	0.970	7.97E-00	0.835
157064	4	4.94E-00	0.971	1.45E-02	1.177	4.96E-00	0.972	5.93E-00	0.836

Table 4.2: [Example 2, $k = 0$] Comparison of the $\mathbb{RT}_0 - \mathbf{P}_0$ mixed approximation with quasi-uniform and adaptive refinements for the convective Brinkman–Forchheimer model with $\rho = 3.5$.

$\mathbb{RT}_1 - \mathbf{P}_1$ scheme with quasi-uniform refinement										
DoF	h	it	$\mathsf{e}(\boldsymbol{\sigma})$	$\mathsf{r}(\boldsymbol{\sigma})$	$\mathsf{e}(\mathbf{u})$	$\mathsf{r}(\mathbf{u})$	$\mathsf{e}(\boldsymbol{\sigma},\mathbf{u})$	$\mathsf{r}(\boldsymbol{\sigma},\mathbf{u})$	Θ	$\mathtt{eff}(\Theta)$
752	0.373	4	1.49E+02	–	7.21E-01	–	1.50E+02	–	2.04E+02	0.736
3040	0.206	4	9.76E+01	0.608	2.14E-01	1.742	9.78E+01	0.612	1.24E+02	0.789
12096	0.103	4	9.06E+01	0.108	1.15E-01	0.903	9.07E+01	0.109	1.10E+02	0.829
47968	0.049	4	3.30E+01	1.469	2.57E-02	2.172	3.30E+01	1.469	4.18E+01	0.788
190688	0.026	4	1.11E+01	1.575	4.28E-03	2.595	1.11E+01	1.575	1.39E+01	0.800
762272	0.013	4	3.01E-00	1.888	6.91E-04	2.633	3.01E-00	1.888	3.76E-00	0.799

$\mathbb{RT}_1 - \mathbf{P}_1$ scheme with adaptive refinement via Θ									
DoF	it	$\mathsf{e}(\boldsymbol{\sigma})$	$\mathsf{r}(\boldsymbol{\sigma})$	$\mathsf{e}(\mathbf{u})$	$\mathsf{r}(\mathbf{u})$	$\mathsf{e}(\boldsymbol{\sigma},\mathbf{u})$	$\mathsf{r}(\boldsymbol{\sigma},\mathbf{u})$	Θ	$\mathtt{eff}(\Theta)$
752	4	1.49E+02	–	7.21E-01	–	1.50E+02	–	2.04E+02	0.736
1500	4	9.94E+01	1.177	1.38E-01	4.794	9.95E+01	1.187	1.23E-02	0.809
2618	4	3.63E+01	3.613	3.16E-02	5.291	3.64E+01	3.615	4.49E+01	0.811
4384	4	9.13E-00	5.361	2.95E-02	0.260	9.16E-00	5.352	1.25E+01	0.734
10446	4	3.91E-00	1.950	1.49E-02	1.576	3.93E-00	1.948	5.20E-00	0.759
22888	4	1.78E-00	2.005	5.67E-03	2.464	1.79E-00	2.006	2.38E-00	0.751
55878	4	7.40E-01	1.972	2.04E-03	2.291	7.42E-01	1.973	9.72E-01	0.763
133520	4	3.21E-01	1.919	7.70E-04	2.236	3.21E-01	1.920	4.25E-01	0.756
351102	4	1.27E-01	1.918	3.19E-04	1.823	1.27E-01	1.918	1.64E-01	0.774

Table 4.3: [Example 2, $k = 1$] Comparison of the $\mathbb{RT}_1 - \mathbf{P}_1$ mixed approximation with quasi-uniform and adaptive refinements for the convective Brinkman–Forchheimer model with $\rho = 3.5$.

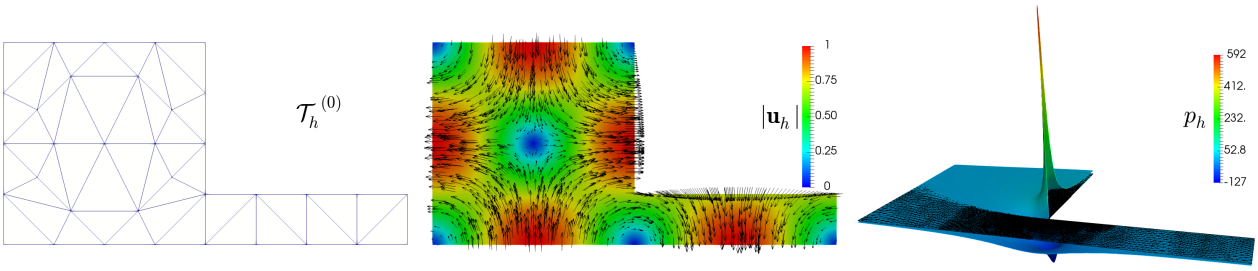

Figure 4.2: [Example 2] Initial mesh, computed magnitude of the velocity, and pressure field.

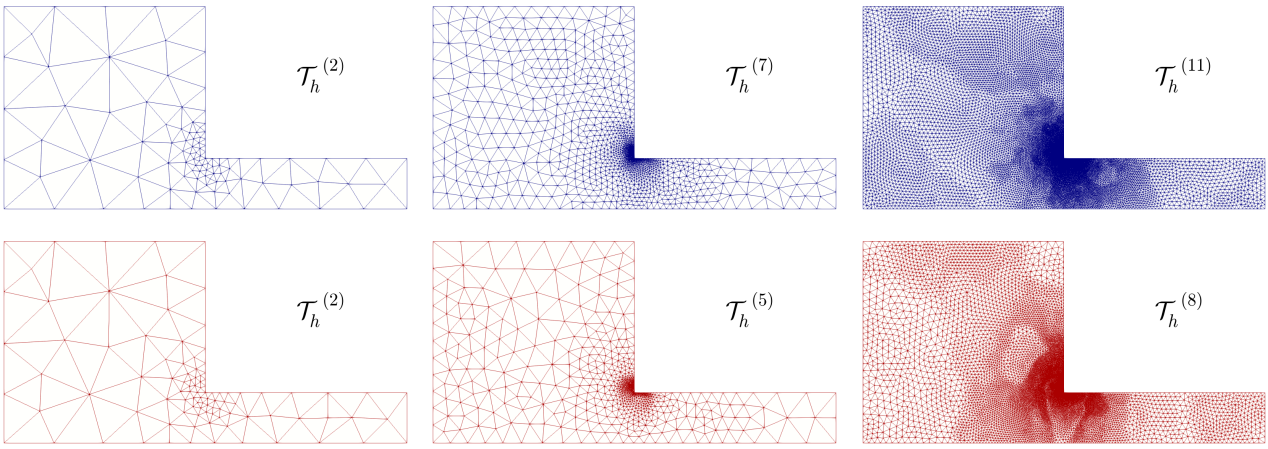

Figure 4.3: [Example 2] Three snapshots of adapted meshes according to the indicator Θ for $k = 0$ and $k = 1$ (top and bottom plots, respectively).

exact solutions given by

$$\mathbf{u}(\mathbf{x}) := \begin{pmatrix} \sin(\pi x_1)\cos(\pi x_2)\cos(\pi x_3) \\ -2\cos(\pi x_1)\sin(\pi x_2)\cos(\pi x_3) \\ \cos(\pi x_1)\cos(\pi x_2)\sin(\pi x_3) \end{pmatrix} \quad \text{and} \quad p(\mathbf{x}) := \frac{10\, x_3}{(x_1 - 0.02)^2 + (x_3 - 0.02)^2} - p_0\,,$$

where $p_0 \in \mathrm{R}$ is a constant chosen in such a way $\int_\Omega p = 0$. Similarly, Table 4.4 along with the Figure 4.4 confirm a disturbed convergence under quasi-uniform refinement and optimal convergence rates when using adaptive refinement guided by the *a posteriori* error estimator Θ. In turn, the initial mesh and approximate solutions built using the adaptive $\mathbb{RT}_0 - \mathbf{P}_0$ scheme (via Θ) with $1,275,474$ degrees of freedom and $139,230$ tetrahedra, are shown in Figure 4.5, whereas snapshots of three meshes via Θ are shown in Figure 4.6 observing a clear clustering of elements around the contraction region.

Example 4: Flow through a 2D porous media with fracture network.

Inspired by [7, Example 3 in Section 6] and [6, Example 4 in Section 6], we finally focus on a flow through a porous medium with a fracture network considering strong jump discontinuities of the parameters `F` and `D` accross the two regions. We consider the square domain $\Omega = (-1,1)^2$ with an internal fracture network denoted as Ω_{f} (see the first plot of Figure 4.7 below), and boundary Γ, whose left, right, upper and lower parts are given by $\Gamma_{\mathrm{left}} = \{-1\} \times (-1,1)$, $\Gamma_{\mathrm{right}} = \{1\} \times$

$\mathbb{RT}_0 - \mathbf{P}_0$ scheme with quasi-uniform refinement										
DoF	h	it	e($\boldsymbol{\sigma}$)	r($\boldsymbol{\sigma}$)	e($\mathbf{u}$)	r($\mathbf{u}$)	e($\boldsymbol{\sigma}, \mathbf{u}$)	r($\boldsymbol{\sigma}, \mathbf{u}$)	Θ	eff(Θ)
1464	0.354	5	1.16E+02	–	8.78E-01	–	1.17E+02	–	1.20E+02	0.977
11040	0.177	5	1.06E+02	0.143	6.08E-01	0.546	1.06E+02	0.145	1.03E+02	1.032
57624	0.101	4	9.40E+01	0.213	4.17E-01	0.683	9.45E+01	0.215	9.00E+01	1.049
285984	0.059	4	7.10E+01	0.527	2.30E-01	1.117	7.12E+01	0.529	6.75E+01	1.055
1518804	0.034	4	4.63E+01	0.767	1.11E-01	1.305	4.64E+01	0.769	4.40E+01	1.055

$\mathbb{RT}_0 - \mathbf{P}_0$ scheme with adaptive refinement via Θ									
DoF	it	e($\boldsymbol{\sigma}$)	r($\boldsymbol{\sigma}$)	e($\mathbf{u}$)	r($\mathbf{u}$)	e($\boldsymbol{\sigma}, \mathbf{u}$)	r($\boldsymbol{\sigma}, \mathbf{u}$)	Θ	eff(Θ)
1464	5	1.16E+02	–	8.78E-01	–	1.17E+02	–	1.20E+02	0.977
5943	5	1.09E+02	0.136	6.62E-01	0.603	1.10E+02	0.139	1.07E+02	1.032
42579	4	9.11E+01	0.277	3.66E-01	0.903	9.15E+01	0.280	8.88E+01	1.030
148755	4	6.13E+01	0.949	1.81E-01	1.686	6.15E+01	0.951	5.84E+01	1.053
1275474	4	2.38E+01	1.322	4.02E-02	2.102	2.38E+01	1.324	2.26E+01	1.053

Table 4.4: [Example 3] Comparison of the $\mathbb{RT}_0 - \mathbf{P}_0$ mixed approximation with quasi-uniform and adaptive refinements for the convective Brinkman–Forchheimer model with $\rho = 4$.

$(-1, 1)$, $\Gamma_{\text{top}} = (-1, 1) \times \{1\}$, and $\Gamma_{\text{bottom}} = (-1, 1) \times \{-1\}$, respectively. Note that the boundary of the internal fracture network is defined as a union of segments. The initial mesh file is available in `https://github.com/scaucao/Fracture_network-mesh`. We consider the convective Brinkman–Forchheimer equations (2.5) in the whole domain Ω, with inertial power $\rho = 3$ but with different values of the parameters `F` and `D` for the interior and the exterior of the fracture, namely

$$\mathtt{F} = \begin{cases} 10 & \text{in} \quad \Omega_{\text{f}} \\ 1 & \text{in} \quad \overline{\Omega} \setminus \Omega_{\text{f}} \end{cases} \quad \text{and} \quad \mathtt{D} = \begin{cases} 1 & \text{in} \quad \Omega_{\text{f}} \\ 1000 & \text{in} \quad \overline{\Omega} \setminus \Omega_{\text{f}} \end{cases} . \tag{4.2}$$

The parameter choice corresponds to increased inertial effect ($\mathtt{F} = 10$) in the fracture and a high permeability ($\mathtt{D} = 1$), compared to reduced inertial effect ($\mathtt{F} = 1$) in the porous medium and low permeability ($\mathtt{D} = 1000$). In turn, the body force term is $\mathbf{f} = \mathbf{0}$ and the boundaries conditions are

$$\boldsymbol{\sigma}\,\mathbf{n} = \begin{cases} (-0.5(x_2 - 1),\, 0)^{\text{t}} & \text{on} \quad \Gamma_{\text{left}}\,, \\ (0,\, -0.5(x_1 - 1))^{\text{t}} & \text{on} \quad \Gamma_{\text{bottom}}\,, \end{cases} \qquad \boldsymbol{\sigma}\,\mathbf{n} = (0,\, 0)^{\text{t}} \quad \text{on} \quad \Gamma_{\text{right}} \cup \Gamma_{\text{top}}\,, \tag{4.3}$$

which drives the flow in a diagonal direction from the left-bottom corner to the right-top corner of the square domain Ω. In Figure 4.7, we display the initial mesh, the computed magnitude of the velocity, velocity gradient tensor, and pseudostress tensor, which were built using the $\mathbb{RT}_1 - \mathbf{P}_1$ scheme on a mesh with $72,774$ triangle elements (actually representing $1,165,408\,\mathtt{DoF}$) obtained via Θ (cf. (3.1)). Similarly to [7, Example 3 in Section 6], we observe that the velocity in the fractures is higher than the velocity in the porous medium, due to the smaller thickness of the fractures and the parameter settings in (4.2). Also, the velocity is higher in branches of the network where the fluid enters from the left-bottom corner and decreases toward the right-top corner of the domain. In addition, we observe a sharp velocity gradient across the interfaces between the fractures and the porous medium. The pseudostress is consistent with the boundary conditions (4.3) and it is more diffused since it includes the pressure field. This example illustrates the ability of the method to provide accurate resolution and numerically stable results for heterogeneous inclusions with high aspect ratio and complex geometry, as presented in the network of thin fractures. These results are in agreement with those reported in [7] but now taking into account that the mesh employed was obtained through an adaptive refinement process

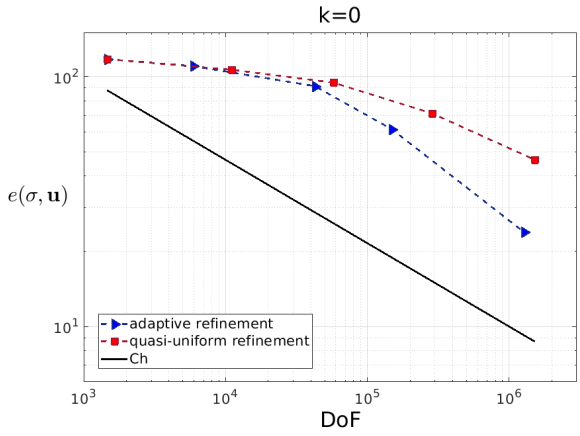

Figure 4.4: [Example 3] Log-log plot of $\mathtt{e}(\boldsymbol{\sigma}, \mathbf{u})$ vs. $\mathtt{DoF}$ for quasi-uniform/adaptive refinements for $k = 0$.

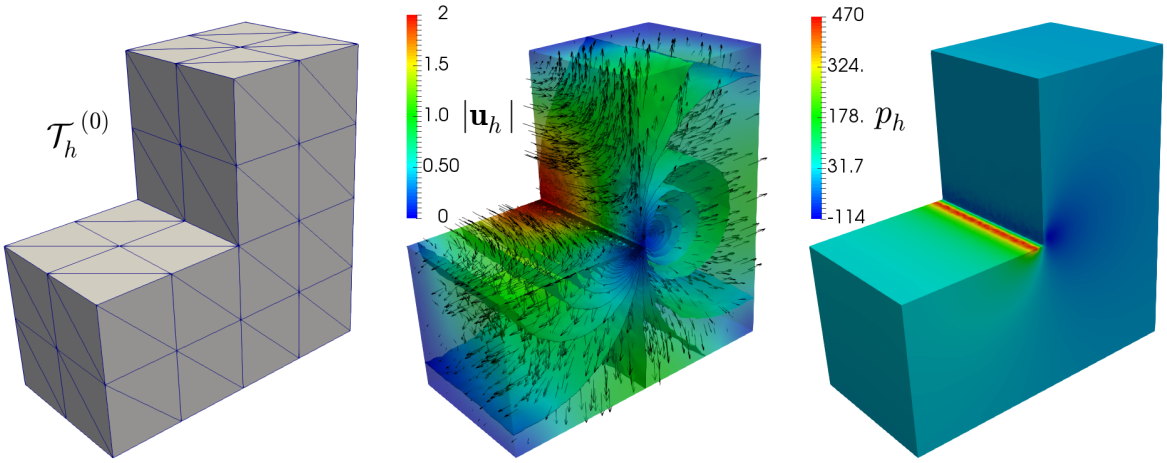

Figure 4.5: [Example 3] Initial mesh, computed magnitude of the velocity, and pressure field.

guided by the *a posteriori* error indicator Θ. In turn, snapshots of some adapted meshes generated using Θ are depicted in Figure 4.8. We can observe a suitable refinement around the interface that couples the porous medium with the fracture network, as well as in the regions where the velocity is higher. This suggests that the indicator Θ is able to detect the strong jump discontinuities of the model parameters along the interface between the fracture and the porous media, as expected, while simultaneously localizing the regions where the solutions are higher.

A Preliminaries for reliability

We start by introducing a few useful notations for describing local information on elements and edges or faces depending on wether $d = 2$ or $d = 3$, respectively. Let $\mathcal{E}_h$ be the set of edges or faces of $\mathcal{T}_h$, whose corresponding diameters are denoted by h_e, and define

$$\mathcal{E}_h(\Omega) := \{e \subseteq \mathcal{E}_h : \quad e \subseteq \Omega\} \quad \text{and} \quad \mathcal{E}_h(\Gamma) := \{e \subseteq \mathcal{E}_h : \quad e \subseteq \Gamma\}.$$

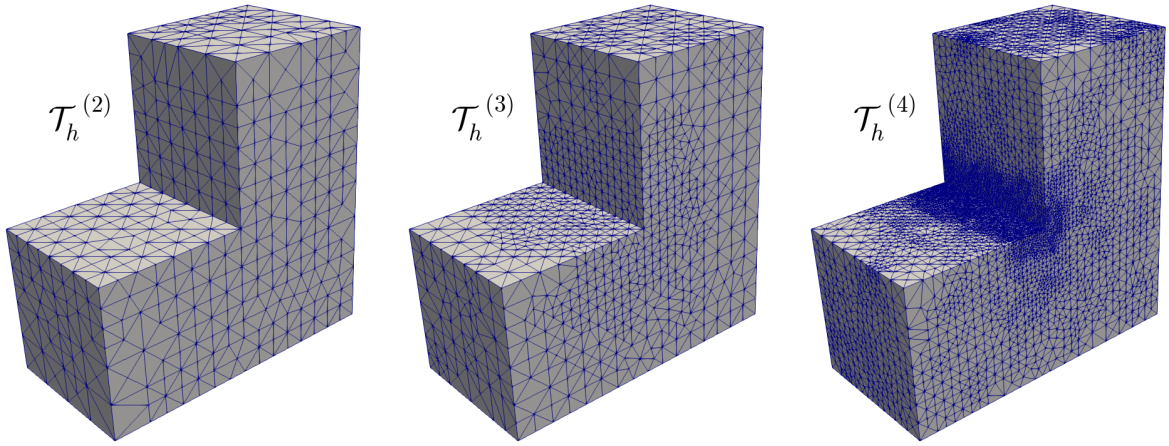

Figure 4.6: [Example 3] Three snapshots of adapted meshes according to the indicator Θ for $k = 0$.

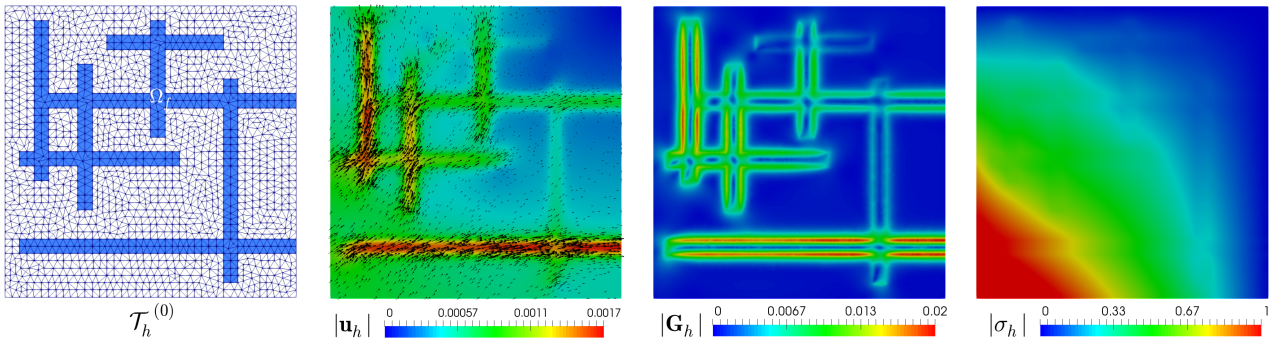

Figure 4.7: [Example 4] Initial mesh, computed magnitude of the velocity, velocity gradient tensor, and pseudostress tensor.

For each $T \in \mathcal{T}_h$, we let $\mathcal{E}_{h,T}$ be the set of edges or faces of T, and denote

$$\mathcal{E}_{h,T}(\Omega) := \{e \subseteq \partial T : \quad e \subseteq \mathcal{E}_h(\Omega)\} \quad \text{and} \quad \mathcal{E}_{h,T}(\Gamma) := \{e \subseteq \partial T : \quad e \subseteq \mathcal{E}_h(\Gamma)\}\,.$$

We also define the unit normal vector $\mathbf{n}_e$ on each edge or face by

$$\mathbf{n}_e := (n_1, \ldots, n_d)^{\mathrm{t}} \quad \forall\, e \in \mathcal{E}_h\,.$$

Hence, when $d = 2$ we can define the tangential vector $\mathbf{s}_e$ by

$$\mathbf{s}_e := (-n_2, n_1)^{\mathrm{t}} \quad \forall\, e \in \mathcal{E}_h\,.$$

However, when no confusion arises, we will simply write $\mathbf{n}$ and $\mathbf{s}$ instead of $\mathbf{n}_e$ and $\mathbf{s}_e$, respectively.

The usual jump operator $[\![\cdot]\!]$ across internal edges or faces is defined for piecewise continuous tensor, vector, or scalar-valued functions $\boldsymbol{\zeta}$, by

$$[\![\boldsymbol{\zeta}]\!] = \big(\boldsymbol{\zeta}|_{T_+}\big)\,|_e - \big(\boldsymbol{\zeta}|_{T_-}\big)\,|_e \quad \text{with} \quad e = \partial T_+ \cap \partial T_-\,, \tag{A.1}$$

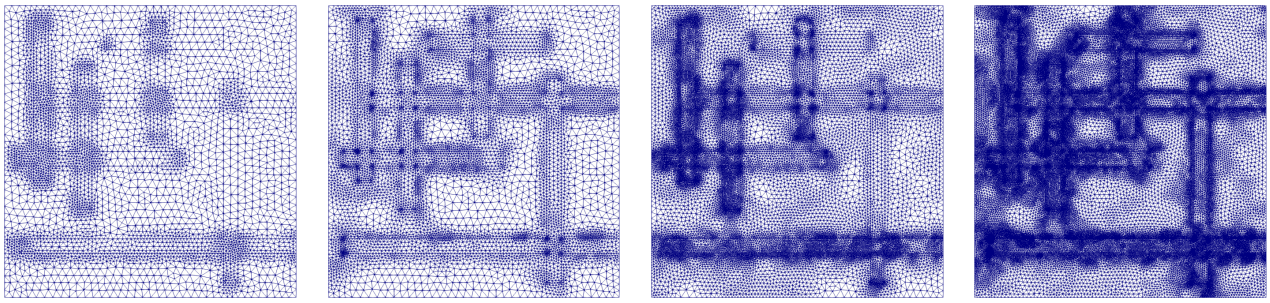

Figure 4.8: [Example 4] Four snapshots of adapted meshes according to the indicator Θ for $k = 1$.

where T_+ and T_- are the elements of $\mathcal{T}_h$ having e as a common edge or face. Finally, for sufficiently smooth vector $\mathbf{v} := (v_1, \ldots, v_d)^{\mathrm{t}}$ and tensor fields $\boldsymbol{\tau} := (\tau_{ij})_{i,j=1,d}$, we let

$$\boldsymbol{\delta}_*(\boldsymbol{\tau}) = \begin{cases} \boldsymbol{\tau}\,\mathbf{s} & , \quad \text{for } d = 2, \\ \begin{pmatrix} (\boldsymbol{\tau}_1^{\mathrm{t}} \times \mathbf{n})^{\mathrm{t}} \\ (\boldsymbol{\tau}_2^{\mathrm{t}} \times \mathbf{n})^{\mathrm{t}} \\ (\boldsymbol{\tau}_3^{\mathrm{t}} \times \mathbf{n})^{\mathrm{t}} \end{pmatrix} & , \quad \text{for } d = 3, \end{cases} \qquad \mathbf{curl}(\mathbf{v}) := \begin{pmatrix} -\dfrac{\partial v_1}{\partial x_2} & \dfrac{\partial v_1}{\partial x_1} \\ -\dfrac{\partial v_2}{\partial x_2} & \dfrac{\partial v_2}{\partial x_1} \end{pmatrix} \quad \text{for } d = 2\,, \tag{A.2}$$

$$\underline{\mathrm{curl}}(\mathbf{v}) := \begin{cases} \dfrac{\partial v_2}{\partial x_1} - \dfrac{\partial v_1}{\partial x_2} & , \quad \text{for } d = 2\,, \\ \nabla \times \mathbf{v} & , \quad \text{for } d = 3\,, \end{cases} \qquad \underline{\mathbf{curl}}(\boldsymbol{\tau}) = \begin{cases} \begin{pmatrix} \underline{\mathrm{curl}}(\boldsymbol{\tau}_1^{\mathrm{t}}) \\ \underline{\mathrm{curl}}(\boldsymbol{\tau}_2^{\mathrm{t}}) \end{pmatrix} & , \quad \text{for } d = 2, \\ \begin{pmatrix} \underline{\mathrm{curl}}(\boldsymbol{\tau}_1^{\mathrm{t}})^{\mathrm{t}} \\ \underline{\mathrm{curl}}(\boldsymbol{\tau}_2^{\mathrm{t}})^{\mathrm{t}} \\ \underline{\mathrm{curl}}(\boldsymbol{\tau}_3^{\mathrm{t}})^{\mathrm{t}} \end{pmatrix} & , \quad \text{for } d = 3, \end{cases} \tag{A.3}$$

where $\boldsymbol{\tau}_i$ is the i-th row of $\boldsymbol{\tau}$ and the derivatives involved are taken in the distributional sense.

Let us now recall the main properties of the Raviart–Thomas and Clément interpolation operators (cf. [18], [15]). We begin by defining for each $p \geq \frac{2\,d}{d+2}$ the spaces

$$\mathbf{H}_p := \Big\{ \boldsymbol{\tau} \in \mathbf{H}(\mathrm{div}_p; \Omega) : \quad \boldsymbol{\tau}|_T \in \mathbf{W}^{1,p}(T) \quad \forall\, T \in \mathcal{T}_h \Big\}\,, \tag{A.4}$$

and

$$\widehat{\mathbf{H}}_h^{\boldsymbol{\sigma}} := \Big\{ \boldsymbol{\tau} \in \mathbf{H}(\mathrm{div}_p; \Omega) : \quad \boldsymbol{\tau}|_T \in \mathbf{RT}_k(T) \quad \forall\, T \in \mathcal{T}_h \Big\}\,. \tag{A.5}$$

In addition, we let $\Pi_h^k : \mathbf{H}_p \to \widehat{\mathbf{H}}_h^{\boldsymbol{\sigma}}$ be the Raviart–Thomas interpolation operator, which is characterized for each $\boldsymbol{\tau} \in \mathbf{H}_p$ by the identities (see, e.g. [18, Section 1.2.7])

$$\int_e (\Pi_h^k(\boldsymbol{\tau}) \cdot \mathbf{n})\, \xi \;=\; \int_e (\boldsymbol{\tau} \cdot \mathbf{n})\, \xi \quad \forall\, \xi \in \mathrm{P}_k(e), \quad \forall\, \text{edge or face } e \text{ of } \mathcal{T}_h\,, \tag{A.6}$$

when $k \geq 0$, and

$$\int_T \Pi_h^k(\boldsymbol{\tau}) \cdot \boldsymbol{\psi} \;=\; \int_T \boldsymbol{\tau} \cdot \boldsymbol{\psi} \quad \forall\, \boldsymbol{\psi} \in \mathbf{P}_{k-1}(T), \quad \forall\, T \in \mathcal{T}_h\,,$$

when $k \geq 1$. In turn, given $q > 1$ such that $1/p + 1/q = 1$, we let

$$\mathrm{H}_h^{\mathbf{u}} := \Big\{ v \in \mathrm{L}^q(\Omega) : \quad v|_T \in \mathrm{P}_k(T) \quad \forall\, T \in \mathcal{T}_h \Big\}\,, \tag{A.7}$$

and recall from [18, Lemma 1.41] that there holds

$$\mathrm{div}\big(\Pi_h^k(\boldsymbol{\tau})\big) = \mathcal{P}_h^k\big(\mathrm{div}(\boldsymbol{\tau})\big) \quad \forall\, \boldsymbol{\tau} \in \mathbf{H}_p\,, \tag{A.8}$$

where $\mathcal{P}_h^k : \mathrm{L}^p(\Omega) \to \mathrm{H}_h^{\mathbf{u}}$ is the usual orthogonal projector with respect to the $\mathrm{L}^2(\Omega)$-inner product, which satisfies the following error estimate (see [18, Proposition 1.135]): there exists a positive constant C_0, independent of h, such that for $0 \leq \ell \leq k+1$ and $1 \leq p \leq \infty$ there holds

$$\|w - \mathcal{P}_h^k(w)\|_{0,p;\Omega} \,\leq\, C_0\, h^\ell\, \|w\|_{\ell,p;\Omega} \quad \forall\, w \in \mathrm{W}^{\ell,p}(\Omega)\,. \tag{A.9}$$

We stress that $\mathcal{P}_h^k(w)|_T = \mathcal{P}_T^k(w|_T)\ \forall\, w \in \mathrm{L}^p(\Omega)$, where $\mathcal{P}_T^k : \mathrm{L}^p(T) \to \mathrm{P}_k(T)$ is the corresponding local orthogonal projector. In addition, denoting by $\mathbf{H}_h^{\mathbf{u}}$ the vector version of $\mathrm{H}_h^{\mathbf{u}}$ (cf. (A.7)), we let $\boldsymbol{\mathcal{P}}_h^k : \mathbf{L}^p(\Omega) \to \mathbf{H}_h^{\mathbf{u}}$ be the vector version of $\mathcal{P}_h^k$.

Next, we collect some approximation properties of Π_h^k.

Lemma A.1 *Given $p > 1$, there exist positive constants C_1, C_2, independent of h, such that for $0 \leq \ell \leq k$ and for each $T \in \mathcal{T}_h$ there holds*

$$\|\boldsymbol{\tau} - \Pi_h^k(\boldsymbol{\tau})\|_{0,p;T} \,\leq\, C_1\, h_T^{\ell+1}\, |\boldsymbol{\tau}|_{\ell+1,p;T} \quad \forall\, \boldsymbol{\tau} \in \mathbf{W}^{\ell+1,p}(T)\,, \tag{A.10}$$

and

$$\|\boldsymbol{\tau}\cdot\mathbf{n} - \Pi_h^k(\boldsymbol{\tau})\cdot\mathbf{n}\|_{0,p;e} \leq C_2\, h_e^{1-1/p}\, |\boldsymbol{\tau}|_{1,p;T} \quad \forall\, \boldsymbol{\tau} \in \mathbf{W}^{1,p}(T), \quad \forall\, e \in \mathcal{E}_h(T)\,. \tag{A.11}$$

Proof. For the estimate (A.10) we refer to [22, Lemma 3.1], whereas the proof of (A.11) can be found in [3, Lemma 4.2]. □

Furthermore, denoting by $\mathbb{H}_p$ and $\widehat{\mathbb{H}}_h^{\boldsymbol{\sigma}}$ the tensor versions of $\mathbf{H}_p$ (cf. (A.4)) and $\widehat{\mathbf{H}}_h^{\boldsymbol{\sigma}}$ (cf. (A.5)), respectively, we let $\boldsymbol{\Pi}_h^k : \mathbb{H}_p \to \widehat{\mathbb{H}}_h^{\boldsymbol{\sigma}}$ be the operator Π_h^k acting row-wise. Then, according to the decomposition (2.6), for each $\boldsymbol{\tau} \in \mathbb{H}_p$ there holds

$$\boldsymbol{\Pi}_h^k(\boldsymbol{\tau}) \,=\, \boldsymbol{\Pi}_{h,0}^k(\boldsymbol{\tau}) + \jmath\,\mathbb{I}, \quad \text{with} \quad \jmath := \frac{1}{d\,|\Omega|}\int_\Omega \mathrm{tr}(\boldsymbol{\Pi}_h^k(\boldsymbol{\tau})) \in \mathrm{R}$$

$$\text{and} \quad \boldsymbol{\Pi}_{h,0}^k(\boldsymbol{\tau}) \,:=\, \boldsymbol{\Pi}_h^k(\boldsymbol{\tau}) - \jmath\,\mathbb{I} \in \mathbb{H}_h^{\boldsymbol{\sigma}}\,.$$

Other approximation properties of Π_h^k and $\boldsymbol{\Pi}_h^k$, in particular those involving the div and **div** operators, and using (A.8) and (A.9), and their tensorial versions with $\boldsymbol{\Pi}_h^k$ and $\boldsymbol{\mathcal{P}}_h^k$, can also be derived.

We now recall from [3, Lemma 4.4] a stable Helmholtz decomposition for the nonstandard Banach space $\mathbb{H}(\mathbf{div}_p;\Omega)$, whose particular case given by $p = 4/3$ is considered in the present paper. More precisely, we have the following result.

Lemma A.2 *Let $1 < p \leq 2$ when $d = 2$ and $6/5 \leq p \leq 2$ when $d = 3$. Then, for each $\boldsymbol{\tau} \in \mathbb{H}(\mathbf{div}_p;\Omega)$, there exist*

(a) $\boldsymbol{\zeta} \in \mathbb{W}^{1,p}(\Omega)$ and $\boldsymbol{\xi} \in \mathbf{H}^1(\Omega)$ such that $\boldsymbol{\tau} = \boldsymbol{\zeta} + \mathbf{curl}(\boldsymbol{\xi})$ in Ω when $d = 2$,

(b) $\boldsymbol{\zeta} \in \mathbb{W}^{1,p}(\Omega)$ and $\boldsymbol{\xi} \in \mathbb{H}^1(\Omega)$ such that $\boldsymbol{\tau} = \boldsymbol{\zeta} + \underline{\mathbf{curl}}(\boldsymbol{\xi})$ in Ω when $d = 3$.

In addition, in both cases there holds

$$\|\boldsymbol{\zeta}\|_{1,p;\Omega} + \|\boldsymbol{\xi}\|_{1,\Omega} \leq C_p\, \|\boldsymbol{\tau}\|_{\mathbf{div}_p;\Omega}\,,$$

where C_p is a positive constant independent of all the foregoing variables.

On the other hand, defining $X_h := \{v_h \in C(\overline{\Omega}) : \quad v_h|_T \in \mathrm{P}_1(T) \quad \forall\, T \in \mathcal{T}_h\}$ and denoting by $\mathbf{X}_h$ its tensor version, we let $\mathcal{I}_h : \mathrm{H}^1(\Omega) \to X_h$ and $\boldsymbol{\mathcal{I}}_h : \mathbb{H}^1(\Omega) \to \mathbf{X}_h$ be the usual Clément interpolation operator and its tensor version, respectively. Some local properties of $\mathcal{I}_h$, and hence of $\boldsymbol{\mathcal{I}}_h$, are established in the following lemma (cf. [15]):

Lemma A.3 *There exist positive constants C_1 and C_2, such that*

$$\|v - \mathcal{I}_h(v)\|_{0,T} \leq C_1\, h_T\, \|v\|_{1,\Delta(T)} \quad \forall\, T \in \mathcal{T}_h\,,$$

and

$$\|v - \mathcal{I}_h(v)\|_{0,e} \leq C_2\, h_e^{1/2}\, \|v\|_{1,\Delta(e)} \quad \forall\, e \in \mathcal{E}_h\,,$$

where $\Delta(T) := \cup\{T' \in \mathcal{T}_h : \quad T' \cap T \neq \emptyset\}$ and $\Delta(e) := \cup\{T' \in \mathcal{T}_h : \quad T' \cap e \neq \emptyset\}$.

B Preliminaries for efficiency

For the efficiency analysis of Θ (cf. (3.1)), we proceed as in [23], [9], [3] and [22], and apply the localization technique based on bubble functions, along with inverse and discrete trace inequalities. For the former, given $T \in \mathcal{T}_h$, we let T be the usual element-bubble function (cf. [30, eqs. (1.5) and (1.6)]), which satisfies

$$\psi_T \in \mathrm{P}_3(T), \quad \mathrm{supp}(\psi_T) \subseteq T, \quad \psi_T = 0 \quad \text{on} \quad \partial T \quad \text{and} \quad 0 \leq \psi_T \leq 1 \quad \text{in} \quad T\,. \tag{B.1}$$

The specific properties of ψ_T to be employed in what follows, are collected in the following lemma, for whose proof we refer to [30, Lemma 3.3 and Remark 3.2].

Lemma B.1 *Let k be a non-negative integer, and let $p, q \in (1, +\infty)$ conjugate to each other, that is such that $1/p + 1/q = 1$, and $T \in \mathcal{T}_h$. Then, there exist positive constants c_1, c_2, and c_3, independent of h and T, but depending on the shape-regularity of the triangulations (minimum angle condition) and k, such that for each $u \in \mathrm{P}_k(T)$ there hold*

$$c_1 \|u\|_{0,p;T} \leq \sup_{0 \neq v \in \mathrm{P}_k(T)} \frac{\displaystyle\int_T u\, \psi_T v}{\|v\|_{0,q;T}} \leq \|u\|_{0,p;T} \tag{B.2}$$

and

$$c_2\, h_T^{-1} \|\psi_T u\|_{0,q;T} \leq \|\nabla(\psi_T u)\|_{0,q;T} \leq c_3\, h_T^{-1} \|\psi_T u\|_{0,q;T}\,. \tag{B.3}$$

In turn, the aforementioned inverse inequality is stated as follows (cf. [24, Lemma 1.138]).

Lemma B.2 *Let k, ℓ, and m be non-negative integers such that $m \leq \ell$, and let $r, s \in [1, +\infty]$, and $T \in \mathcal{T}_h$. Then, there exists $c > 0$, independent of h, T, r, and s, but depending on k, ℓ, m, and the shape regularity of the triangulations, such that*

$$\|v\|_{\ell,r;T} \leq c\, h_T^{m-\ell+d(1/r-1/s)} \|v\|_{m,s;T} \quad \forall\, v \in \mathrm{P}_k(T)\,. \tag{B.4}$$

Finally, proceeding as in [1, Theorem 3.10], that is employing the usual scaling estimates with respect to a fixed reference element $\widehat{T}$, and applying the trace inequality in $\mathrm{W}^{1,p}(\widehat{T})$, for a given $p \in (1, +\infty)$, one is able to establish the following discrete trace inequality.

Lemma B.3 *Let $p \in (1, +\infty)$. Then, there exits $c > 0$, depending only on the shape regularity of the triangulations, such that for each $T \in \mathcal{T}_h$ and $e \in \mathcal{E}(T)$, there holds*

$$\|v\|_{0,p;e}^p \leq c \left\{ h_T^{-1}\, \|v\|_{0,p;T}^p + h_T^{p-1}\, |v|_{1,p;T}^p \right\} \quad \forall\, v \in \mathrm{W}^{1,p}(T)\,. \tag{B.5}$$

References

[1] S. Agmon, *Lectures on Elliptic Boundary Value Problems*. Van Nostrand, Princeton, NJ, 1965.

[2] J. Camaño, C. García, and R. Oyarzúa, *Analysis of a momentum conservative mixed-FEM for the stationary Navier–Stokes problem*. Numer. Methods Partial Differential Equations 37 (2021), no. 5, 2895–2923.

[3] J. Camaño, S. Caucao, R. Oyarzúa, and S. Villa-Fuentes, *A posteriori error analysis of a momentum conservative Banach spaces based mixed-FEM for the Navier–Stokes problem*. Appl. Numer. Math. 176 (2022), 134–158.

[4] J. Camaño, G.N. Gatica, R. Oyarzúa, and G. Tierra, *An augmented mixed finite element method for the Navier-Stokes equations with variable viscosity*. SIAM J. Numer. Anal. 54 (2016), no. 2, 1069–1092.

[5] S. Caucao, M. Discacciati, G.N. Gatica, and R. Oyarzúa, *A conforming mixed finite element method for the Navier–Stokes/Darcy–Forchheimer coupled problem*. ESAIM Math. Model. Numer. Anal. 54 (2020), no. 5, 1689–1723.

[6] S. Caucao and J. Esparza, *An augmented mixed FEM for the convective Brinkman–Forchheimer problem: a priori and a posteriori error analysis*. J. Comput. Appl. Math. 438 (2024), Paper No. 115517, 27 pp.

[7] S. Caucao, G.N. Gatica, and L.F. Gatica, *A Banach spaces-based mixed finite element method for the stationary convective Brinkman–Forchheimer problem*. Calcolo 60 (2023), no. 4, Paper No. 51, 32 pp.

[8] S. Caucao, G.N. Gatica, and J.P. Ortega, *A posteriori error analysis of a Banach spaces-based fully mixed FEM for double-diffusive convection in a fluid-saturated porous medium*. Computational Geosciences. 27 (2023), no. 2, 289–316.

[9] S. Caucao, G.N. Gatica, R. Oyarzúa, and F. Sandoval, *Residual-based a posteriori error analysis for the coupling of the Navier–Stokes and Darcy–Forchheimer equations*. ESAIM: Math. Model. Numer. Anal. 55 (2021), no. 2, 659–687.

[10] S. Caucao, G.N. Gatica, R. Oyarzúa, and P. Zúñiga, *A posteriori error analysis of a mixed finite element method for the coupled Brinkman–Forchheimer and double-diffusion equations*. J. Sci. Comput. 93 (2022), no. 2, Paper No. 50, 42 pp.

[11] S. Caucao, D. Mora, and R. Oyarzúa, *A priori and a posteriori error analysis of a pseudostress-based mixed formulation of the Stokes problem with varying density*. IMA J. Numer. Anal. 36 (2016), no. 2, 947–983.

[12] S. Caucao, R. Oyarzúa, and S. Villa-Fuentes, *A new mixed-FEM for steady-state natural convection models allowing conservation of momentum and thermal energy*. Calcolo 57 (2020), no. 4, Paper No. 36, 39 pp.

[13] S. Caucao, R. Oyarzúa, and S. Villa-Fuentes, *A posteriori error analysis of a momentum and thermal energy conservative mixed-FEM for the Boussinesq equations*. Calcolo 59 (2022), no. 4, Paper No. 45, 40 pp.

[14] A.O. Celebi, V.K. Kalantarov, and D. Ugurlu, *Continuous dependence for the convective Brinkman–Forchheimer equations*. Appl. Anal. 84 (2005), no. 9, 877–888.

[15] P. Clément, *Approximation by finite element functions using local regularisation*. RAIRO Modélisation Mathématique et Analyse Numérique 9 (1975), 77–84.

[16] C.I. Correa and G.N. Gatica, *On the continuous and discrete well-posedness of perturbed saddle-point formulations in Banach spaces*. Comput. Math. Appl. 117 (2022), 14–23.

[17] C. Domínguez, G.N. Gatica, and S. Meddahi, *A posteriori error analysis of a fully-mixed finite element method for a two-dimensional fluid-solid interaction problem*. J. Comput. Math. 33 (2015), no. 6, 606–641.

[18] A. Ern and J.-L. Guermond, *Theory and Practice of Finite Elements*. Applied Mathematical Sciences, 159. Springer-Verlag, New York, 2004.

[19] V.J. Ervin and T.N. Phillips, *Residual a posteriori error estimator for a three-field model of a non-linear generalized Stokes problem*. Comput. Methods Appl. Mech. Engrg. 195 (2006), no. 19-22, 2599–2610.

[20] M. Farhloul and A.M. Zine, *A posteriori error estimation for a dual mixed finite element approximation of non-Newtonian fluid flow problems*. Int. J. Numer. Anal. Model. 5 (2008), no. 2, 320–330.

[21] G.N. Gatica, *A Simple Introduction to the Mixed Finite Element Method. Theory and Applications*. SpringerBriefs in Mathematics. Springer, Cham, 2014.

[22] G.N. Gatica, C. Inzunza, R. Ruiz-Baier, and F. Sandoval, *A posteriori error analysis of Banach spaces-based fully-mixed finite element method for Boussinesq-type models*. J. Numer. Math. 30 (2022), no. 4, 325–356.

[23] G.N. Gatica, A. Márquez, and M.A. Sánchez, *Analysis of a velocity-pressure-pseudostress formulation for the stationary Stokes equations*. Comput. Methods Appl. Mech. Engrg. 199 (2010), 1064–1079.

[24] V. Girault and P.A. Raviart, *Finite Element Methods for Navier–Stokes Equations. Theory and Algorithms*. Springer Series in Computational Mathematics, 5. Springer-Verlag, Berlin, 1986.

[25] R. Glowinski and A. Marrocco, *Sur l'approximation, par éléments finis d'ordre un, et la résolution, par pénalisations-dualité d'une classe de problémes de Dirichlet non lineaires*. R.A.I.R.O. tome 9, no 2 (1975), p. 41-76.

[26] F. Hecht, *New development in FreeFem++*. J. Numer. Math. 20 (2012), 251-–265.

[27] F. Hecht, *Freefem++*. Third Edition, Version 3.58-1. Laboratoire Jacques-Louis Lions, Université Pierre et Marie Curie, Paris, 2018. [available in `http://www.freefem.org/ff++`].

[28] D. Liu and K. Li, *Mixed finite element for two-dimensional incompressible convective Brinkman-Forchheimer equations*. Appl. Math. Mech. (English Ed.) 40 (2019), no. 6, 889–910.

[29] T. Sayah, *A posteriori error estimates for the Brinkman-Darcy-Forchheimer problem*. Comput. Appl. Math. 40 (2021), no. 7, Paper No. 256, 38 pp.

[30] R. Verfürth, *A Review of A-Posteriori Error Estimation and Adaptive Mesh-Refinement Techniques*. Wiley Teubner, Chichester, 1996.

[31] H. Yu, *Axisymmetric solutions to the convective Brinkman-Forchheimer equations*. J. Math. Anal. Appl. 520 (2023), no. 2, Paper No. 126892, 12 pp.

[32] C. Zhao and Y. You, *Approximation of the incompressible convective Brinkman–Forchheimer equations*. J. Evol. Equ. 12 (2012), no. 4, 767–788.

Centro de Investigación en Ingeniería Matemática (CI^{2}MA)

PRE-PUBLICACIONES 2024

2024-07 Raimund Bürger, Enrique D. Fernández Nieto, Jorge Moya: *A multilayer shallow water model for tsunamis and coastal forest interaction*

2024-08 Fernando Betancourt, Raimund Bürger, Stefan Diehl, María Carmen Martí, Yolanda Vásquez: *A degenerating convection-diffusion model of a flotation column: theory, numerics and applications*

2024-09 Fernando Betancourt, Raimund Bürger, Julio Careaga, Lucas Romero: *Coupled finite volume methods for settling in inclined vessels with natural convection*

2024-10 Kaïs Ammari, Vilmos Komornik, Mauricio Sepúlveda, Octavio Vera: *Stability of the Rao-Nakra sandwich beam with a dissipation of fractional derivative type: theoretical and numerical study*

2024-11 Lady Angelo, Jessika Camaño, Sergio Caucao: *A skew-symmetric-based mixed FEM for stationary MHD ows in highly porous media*

2024-12 Gabriel N. Gatica: *A note on the generalized Babuska-Brezzi theory: revisiting the proof of the associated Strang error estimates*

2024-13 Carlos D. Acosta, Raimund Bürger, Julio Careaga, Stefan Diehl, Romel Pineda, Daniel Támara: *A semi-implicit method for a degenerating convection-diffusion-reaction problem modeling secondary settling tanks*

2024-14 Gabriel N. Gatica, Cristian Inzunza, Ricardo Ruiz-Baier: *Primal-mixed finite element methods for the coupled Biot and Poisson-Nernst-Planck equations*

2024-15 Isaac Bermudez, Víctor Burgos, Jessika Camaño, Fernando Gajardo, Ricardo Oyarzúa, Manuel Solano: *Mixed finite element methods for coupled fluid flow problems arising from reverse osmosis modeling*

2024-16 Mario Álvarez, Gonzalo A. Benavides, Gabriel N. Gatica, Esteban Henriquez: *Banach spaces-based mixed finite element methods for a steady sedimentation-consolidation system*

2024-17 Tomás Barrios, Edwin Behrens, Rommel Bustinza, Jose M. CASCON: *An a posteriori error estimator for an augmented variational formulation of the Brinkman problem with mixed boundary conditions and non-null source terms*

2024-18 Sergio Caucao, Gabriel N. Gatica, Luis F. Gatica: *A posteriori error analysis of a mixed finite element method for the stationary convective Brinkman–Forchheimer problem*

Para obtener copias de las Pre-Publicaciones, escribir o llamar a: Director, Centro de Investigación en Ingeniería Matemática, Universidad de Concepción, Casilla 160-C, Concepción, Chile, Tel.: 41-2661324, o bien, visitar la página web del centro: http://www.ci2ma.udec.cl







Centro de Investigación en
Ingeniería Matemática (CI²MA)
Universidad de Concepción

Casilla 160-C, Concepción, Chile
Tel.: 56-41-2661324/2661554/2661316
http://www.ci2ma.udec.cl